The Astrophysical Journal, 987:23 (20pp), 2025 July 1 https://doi.org/10.3847/1538-4357/add25f

"Oh FUors, Where Art Thou?": A Search for Long-lasting Young Stellar Object Outbursts Hiding in Infrared Surveys

Carlos Contreras Peña[1,2], Jeong-Eun Lee[1,3], Ho-Gyu Lee[4], Gregory Herczeg[5,6], Doug Johnstone[7,8], Hanpu Liu[5,6], Philip W. Lucas[9], Zhen Guo[9,10,11], Michael A. Kuhn[9], Leigh C. Smith[12], Mizna Ashraf[13], Jessy Jose[13], Sung-Yong Yoon[4,14], and Sung-Chul Yoon[1]

[1] Department of Physics and Astronomy, Seoul National University, 1 Gwanak-ro, Gwanak-gu, Seoul 08826, Republic of Korea; cecontrep@gmail.com, ccontreras@snu.ac.kr
[2] Research Institute of Basic Sciences, Seoul National University, Seoul 08826, Republic of Korea
[3] SNU Astronomy Research Center, Seoul National University, 1 Gwanak-ro, Gwanak-gu, Seoul 08826, Republic of Korea
[4] Korea Astronomy and Space Science Institute, 776 Daedeok-daero, Yuseong, Daejeon 34055, Republic of Korea
[5] Kavli Institute for Astronomy and Astrophysics, Peking University, Yiheyuan Lu 5, Haidian Qu, 100871 Beijing, People's Republic of China
[6] Department of Astronomy, Peking University, Yiheyuan 5, Haidian Qu, 100871 Beijing, People's Republic of China
[7] NRC Herzberg Astronomy and Astrophysics, 5071 West Saanich Road, Victoria, BC, V9E 2E7, Canada
[8] Department of Physics and Astronomy, University of Victoria, Victoria, BC, V8P 5C2, Canada
[9] Centre for Astrophysics Research, University of Hertfordshire, College Lane, Hatfield, AL10 9AB, UK
[10] Instituto de Fisica y Astronomia, Universidad de Valparaiso, Ave. Gran Bretaña, 1111, Casilla 5030, Valparaiso, Chile
[11] Millennium Institute of Astrophysics, Nuncio Monseñor Sotero Sanz 100, Of. 104, Providencia, Santiago, Chile
[12] Institute of Astronomy, University of Cambridge, Madingley Road, Cambridge CB3 0HA, UK
[13] Department of Physics, Indian Institute of Science Education and Research Tirupati, Yerpedu, Tirupati-517619, Andhra Pradesh, India
[14] School of Space Research, Kyung Hee University, 1732, Deogyeong-daero, Giheung-gu, Yongin-si, Gyeonggi-do 17104, Republic of Korea
Received 2025 February 18; revised 2025 April 28; accepted 2025 April 28; published 2025 June 24

Abstract

Long-lasting episodes of high accretion can strongly impact stellar and planetary formation. However, the universality of these events during the formation of young stellar objects (YSOs) is still under debate. Accurate statistics of strong outbursts (FUors) are necessary to understand the role of episodic accretion bursts. In this work, we search for a population of FUors that may have gone undetected in the past because they either (a) went into outburst before the start of modern monitoring surveys and are now slowly fading back into quiescence or (b) are slow-rising outbursts that would not commonly be classified as candidate FUors. We hypothesize that the light curves of these outbursts should be well fitted by linear models with negative (declining) or positive (rising) slopes. The analysis of the infrared light curves and photometry of ~99,000 YSO candidates from SPICY yields 717 candidate FUors. Infrared spectroscopy of 20 candidates, from both the literature and obtained by our group, confirms that 18 YSOs are going through long-term outbursts and identifies two evolved sources as contaminants. The number of candidate FUors combined with previously measured values of the frequency of FUor outbursts yields average outburst decay times that are 2.5 times longer than the rise times. In addition, a population of outbursts with rise timescales between 2000 and 5000 days must exist to obtain our observed number of YSOs with positive slopes. Finally, we estimate a mean-burst lifetime of between 45 and 100 yr.

Unified Astronomy Thesaurus concepts: Young stellar objects (1834); Protostars (1302); Eruptive variable stars (476); FU Orionis stars (553)

Materials only available in the online version of record: machine-readable table

1. Introduction

In the episodic accretion model of star formation, stars gain most of their mass in short-lived episodes of high accretion followed by long periods of quiescent, low-level accretion (see, e.g., M. L. Enoch et al. 2009; J. Bae et al. 2014; M. M. Dunham et al. 2014; W. J. Fischer et al. 2023). Episodic accretion can have lasting effects on both stellar and planetary formation. It has been invoked as one of the solutions to the observed spread in the luminosities of Class I young stellar objects (YSOs; e.g., S. J. Kenyon et al. 1990; N. J. Evans et al. 2009). The long time spent at high-accretion rates can have long-term effects on the structure of the central star (e.g., I. Baraffe et al. 2017; M. Kunitomo et al. 2017). The associated outbursts can alter the chemistry of protoplanetary disks and envelopes (J.-E. Lee 2007; J. K. Jørgensen et al. 2013; L. Zwicky et al. 2024), move the location of the snowline of various ices (L. A. Cieza et al. 2016; J.-E. Lee et al. 2019), aid in the formation of planetary systems similar to the solar system (A. Hubbard 2017), and affect the orbital evolution of planets, if present (A. P. Boss 2013; J. C. Becker et al. 2021). Despite all these possibilities, however, the role of episodic accretion in stellar mass assembly is still uncertain.

A class of YSOs, known as eruptive variable YSOs (a.k.a. FUors/EX Lup–like), display high-amplitude variability due to a large increase in the accretion rate onto the central star, supporting the episodic accretion model. The most extreme of these outbursts in YSOs, known as FUors after the prototype FU Ori, have accretion rates that increase from normal T Tauri rates of 10^{-8}–$10^{-9}\,M_\odot\,\mathrm{yr}^{-1}$ to reach as high as $10^{-4}\,M_\odot\,\mathrm{yr}^{-1}$, and last for centuries (L. Hartmann & S. J. Kenyon 1996). FUors are detected and classified according to the photometric and spectroscopic characteristics of the outbursts.

The discovery of additional FUors typically requires the observation of a sudden and large amplitude outburst, similar to the brightness changes observed in known FUors, such as FU Ori (G. H. Herbig 1966, 1977), HBC722 (E. H. Semkov et al. 2010), or the majority of newly discovered FUors from the VVV survey (Z. Guo et al. 2024a). This requirement, however, fails to allow for sources that are already undergoing high-accretion outbursts. First, after reaching maximum brightness, FUor outbursts slowly decay over the next ∼10–100 yr. For example, the brightness of FU Ori has been declining since its outburst in 1936 at an average rate of 0.015 mag yr^{-1} (S. J. Kenyon et al. 2000). Thus, if the start of a monitoring campaign misses the outburst in a particular YSO, the slow declining light curve would not be identified as a potential candidate FUor. Second, long-term rising outbursts (such as SSTgbs J21470601+4739394, M. Ashraf et al. 2024) might not be immediately recognized as being driven by large changes in the accretion rate. Therefore, there should exist a population of FUors that remain undetected by the standard discovery criterion.

The confirmation as a bona fide FUor requires a spectroscopic follow-up, as these objects display unique characteristics during the outburst (L. A. Hillenbrand et al. 2019b; A. C. Rodriguez & L. A. Hillenbrand 2022). For example, the near-infrared spectrum of FUors shows a triangular shape *H*-band continuum due to H_2O absorption and strong first overtone ^{12}CO absorption at 2.3–2.4 μm (e.g., M. S. Connelley & B. Reipurth 2018). Hydrogen emission lines, a common feature in YSOs, are usually weak or not present in the spectrum of FUors (M. S. Connelley & T. P. Greene 2010; W. J. Fischer et al. 2012). These features are explained by a rapidly accreting disk that outshines the central protostar at all wavelengths. The absorption lines form in a disk that is heated from the midplane and has a cooler atmosphere (e.g., N. Calvet et al. 1991; L. Hartmann & S. J. Kenyon 1996).

The unique spectroscopic characteristics of FUor outbursts have allowed for the classification of FUor-like sources (see, e.g., R. Mundt et al. 1985; B. Reipurth & C. Aspin 1997; M. S. Connelley & T. P. Greene 2010). These YSOs show the same spectroscopic features as FUors, but where no outburst has been recorded. As FUors have short rise times compared with the expected lifetime in the bright state, outbursts in FUor-like sources likely would have occurred before the start of active monitoring of star-forming regions (SFRs). FUor-like sources are often discovered through spectroscopic studies of stars with particularly interesting properties (such as sources driving Herbig–Haro flows; B. Reipurth & C. Aspin 1997), but these have been mostly serendipitous discoveries while observing samples of YSOs (e.g., G. Sandell & C. Aspin 1998).

Over the last 15 yr, multiepoch, optical (Gaia, Zwicky Transient Facility, Pan-STARRS, and ASSASN; K. C. Chambers et al. 2016; E. C. Bellm et al. 2018; T. Jayasinghe et al. 2018; S. T. Hodgkin et al. 2021), near-IR (UKIRT Infrared Deep Sky Survey: Galactic Plane Survey, hereafter GPS; The VISTA Variables in the Via Lactea survey, hereafter VVV; The Palomar Gattini-IR survey, hereafter PGIR; P. W. Lucas et al. 2008; R. K. Saito et al. 2012; A. M. Moore et al. 2016), mid-IR (Spitzer and Wide-field Infrared Survey Explorer, hereafter WISE and NEOWISE; R. A. Benjamin et al. 2003; E. L. Wright et al. 2010; A. Mainzer et al. 2014), and submillimeter (James Clerk Maxwell Telescope; Y.-H. Lee et al. 2021a; S. Mairs et al. 2024) surveys have led to an increase in the observations of all type of variables, including the rare detection of high-amplitude, long-lasting outbursts (L. A. Hillenbrand et al. 2018; Z. Guo et al. 2021, 2024a; P. W. Lucas et al. 2024). FUor and FUor-like YSOs, however, are still a rare class of variable stars, with roughly ∼50 objects classified as such over the last 85 yr (M. S. Connelley & B. Reipurth 2018; W. J. Fischer et al. 2023). The lack of continuous, long-term monitoring in SFRs can partly explain the scarcity of FUor detection. In addition, until recently, monitoring has been done mostly at optical wavelengths, therefore looking at more evolved YSOs where the rate of FUor outbursts is low (C. Contreras Peña et al. 2019). Observational and theoretical studies suggest that FUor outbursts are more frequent during the earlier Class 0 and Class I stages of young stellar evolution (J. Bae et al. 2014; C. Contreras Peña et al. 2019; W. J. Fischer et al. 2019; T.-H. Hsieh et al. 2019; W. Park et al. 2021; W. Zakri et al. 2022; C. Contreras Peña et al. 2024). YSOs at these stages are usually invisible at optical wavelengths and more readily observed at wavelengths longer than 1 μm.

Accurate statistics of FUor outbursts are critical to understanding the episodic accretion phenomena. In this paper, we aim to detect a population of FUors that may have gone undetected in the past by analyzing the multiepoch near- to mid-IR photometric data of the objects in the Spitzer/IRAC Candidate YSO (SPICY) Catalog for the inner Galactic midplane (M. A. Kuhn et al. 2021). In Section 2, we provide a description of the YSO sample and the multiepoch near- to mid-IR surveys that will be used in our analysis. Section 3 shows the method that is used to classify light curves with the goal of detecting long-term rises and decays that might be associated with FUors. In Section 3.1, we describe the characteristics of 717 candidate FUors that arise from the analysis of Section 3. In addition, in Section 3.2, we present a discussion on possible sources of contamination. Section 4 describes the follow-up observations of a subsample of candidate FUors. Section 5 contains the discussion of the spectroscopic data and the confirmation of the majority of this sample as eruptive YSOs. Using the results of our analysis, we provide, in Section 6, some insights into the timescales involved in FUor outbursts. Finally, Section 7 summarizes our results.

2. Detecting FUors

The number of FUor outbursts that we can detect depends both on the number of YSOs and on the amount of time that this sample is monitored (L. A. Hillenbrand & K. P. Findeisen 2015; C. Contreras Peña et al. 2019). In this work, we attempt to maximize these variables by (1) using the largest available catalog of YSOs, the SPICY Catalog for the inner Galactic midplane (M. A. Kuhn et al. 2021), and (2) using the multiepoch (9–12 yr) near- to mid-IR observations from the Vista Variables in the Via Lactea survey and its extension (VVV/VVVX), and WISE.

2.1. The Sample

To develop the SPICY catalog, M. A. Kuhn et al. (2021) used a random forest classification to select YSOs from Spitzer photometry obtained during the cryogenic mission. This includes seven Spitzer/IRAC surveys covering 613 deg^2.

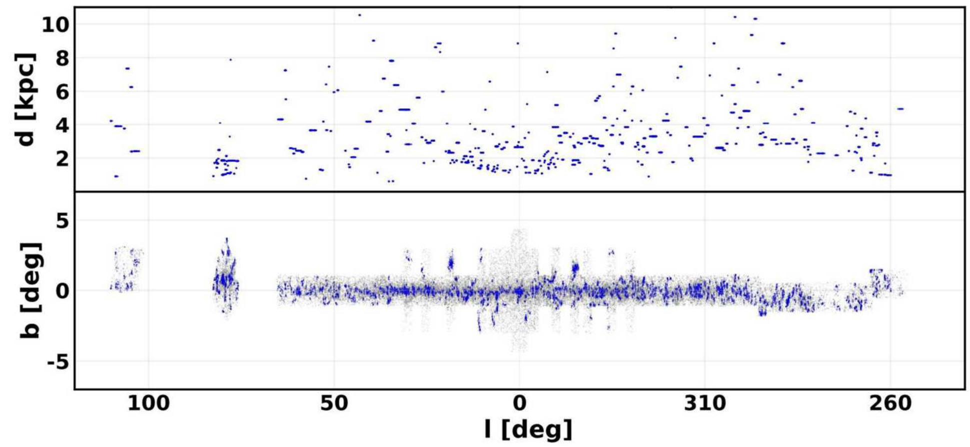

Figure 1. (Top) Distance vs. Galactic longitude for SPICY sources with available distance information. (Bottom) Galactic latitude vs. longitude of SPICY sources (gray dots). Objects with available distance measurements are marked with blue dots.

Their selection is also augmented with three near-infrared surveys: Two Micron All Sky Survey (2MASS; M. F. Skrutskie et al. 2006), UKIDSS Galactic Plane Survey (A. Lawrence et al. 2007; P. W. Lucas et al. 2008), and VVV (R. K. Saito et al. 2012). The SPICY catalog contains 117,446 YSO candidates.

The spectral energy distribution (SED) of YSOs at wavelengths between $2 < \lambda < 24\,\mu$m is generally used to determine the evolutionary stage of the system (e.g., C. J. Lada 1987; M. M. Dunham et al. 2014). The different YSO Classes or stages are defined according to the value of their infrared spectral index, α, defined as

$$\alpha = \frac{d\log(\lambda F_\lambda)}{d\log\lambda}, \tag{1}$$

from which objects are classified as either Class 0, I, II, or flat-spectrum (FS) YSOs (C. J. Lada 1987; P. Andre et al. 1993; T. P. Greene et al. 1994).

Since the value of α estimated using Equation (1) can be affected by reddening, M. A. Kuhn et al. (2021) use 4.5–24 (from Spitzer) or 4.5–22 μm (from Spitzer and WISE) colors to derive α in their sample. M. A. Kuhn et al. (2021) find 15,943 (14% of the sample) Class I ($\alpha > 0.3$), 23,810 (20%) FS ($-0.3 < \alpha < 0.3$), 59,949 (51%) Class II ($-1.6 < \alpha < -0.3$), and 5352 (5%) Class III ($\alpha < -1.6$) YSOs, with an additional 12,392 (10%) YSOs having uncertain classification. For the purposes of this work, we select YSOs classified as either Class I, Class II, or FS sources, reducing the sample to 99,702 sources.

The overall sample of YSOs is distributed within the area covered by the Spitzer surveys, but with a higher density toward the Galactic midplane and some stellar associations (such as the Cygnus-X SFR at $l \sim 78°$; see Figure 1). Information on typical distances for the YSOs in our sample can be determined from the mean parallax of stellar associations found by M. A. Kuhn et al. (2021). 47,218 YSOs are associated with such stellar groups. Figure 1 shows that the majority of the sample is located at distances larger than 0.6 kpc and with a median value of 2.8 kpc.

2.2. WISE

This work uses mid-IR photometry from all-sky observations of the WISE telescope. WISE surveyed the entire sky in four bands, W1 (3.4 μm), W2 (4.6 μm), W3 (12 μm), and W4 (22 μm), with the spatial resolutions of 6.″1, 6.″4, 6.″5, and 12″, respectively, from 2010 January to September (E. L. Wright et al. 2010). The survey continued as the NEOWISE Post-Cryogenic Mission, using only the W1 and W2 bands, for an additional 4 months (A. Mainzer et al. 2011). In 2013 September, WISE was reactivated as the NEOWISE-reactivation (NEOWISE-R) mission (A. Mainzer et al. 2014). NEOWISE-R stopped operating in 2024, and the latest released data set contains observations until 2024 July 31. For each visit to a particular area of the sky, WISE performs several photometric observations over a period of ∼a few days. Each area of the sky is observed similarly every ∼6 months.

For the analysis of SPICY YSOs, we used all the available data from the WISE telescope for observations from 2010 until 2021. The single-epoch data were collected from the NASA/IPAC Infrared Science Archive catalogs using a 3″ radius from the coordinates of the YSO. For each source, we averaged the single-epoch data taken over a few days to produce one epoch of photometry every 6 months (following the procedures described by W. Park et al. 2021).

From the 99,702 SPICY sources in our sample (Section 2.1), we find 53,662 objects (or 54% of the sample) with WISE data (defined as having more than three epochs in W1 or W2 bands).

2.3. VVV/VVVX

For YSOs located in the area covered by the VVV survey and its extension (VVV/VVVX), we also use a preliminary version of the VVV/VIRAC2 catalog (L. C. Smith et al. 2018, 2025). The catalog contains the Z, Y, J, H, and K_s profile fitting photometry from the 2010 through 2019 observations for ∼500 million sources located in the original region covered by the VVV survey (D. Minniti et al. 2010). The astrometric properties of the VISTA K_s data also allow us to determine proper motions and parallaxes for VVV sources. The point-spread function photometry is derived using DoPHOT (P. L. Schechter et al. 1993; J. Alonso-Garcìa et al. 2012), where a new absolute photometric calibration is obtained to mitigate issues that arise from blending of VVV sources in 2MASS data of crowded inner Galactic bulge regions (G. Hajdu et al. 2020; L. C. Smith et al. 2025).

The VIRAC2 catalog also provides values for the proper motions of individual sources, which are calibrated using the Gaia absolute reference frame. Using the proper motions, probability density functions for stellar distance can be estimated using the method described in Z. Guo et al. (2021) by adopting a Galactic rotation curve.

We have photometric information from the VIRAC2 catalog for 32,092 objects (32%). Combined, 16,546 sources (17%) have WISE+VIRAC2 data. An inspection of VIRAC2 sources with no WISE counterparts reveals that they tend to have fainter K_s magnitudes than those sources with WISE+VIRAC2 data. It is likely that fainter sources fall below the detection limits of the WISE telescope.

3. Classification of Light Curves

We identify candidate FUors either with slow-rising outbursts or showing evidence of continual dimming after reaching their peak brightness. For this purpose, we use the methods developed by W. Park et al. (2021) to characterize the NEOWISE light curves.

W. Park et al. (2021) search for secular and stochastic variability in the long-term data of ∼7000 YSOs. Candidate variable stars are selected if they show $\Delta W2/\sigma_{W2} \geqslant 3$.[15] Lomb–Scargle periodogram (LSP; N. R. Lomb 1976; J. D. Scargle 1989), and linear fits are used to search for secular trends in the light curves of candidate variable stars. To quantify the uncertainty in a particular LSP peak or best-fit linear slope, W. Park et al. (2021) define a false alarm probability (FAP) following the method developed by R. V. Baluev (2008) and the methods used in the analysis of submillimeter light curves by Y.-H. Lee et al. (2021a). YSOs that are well fitted by a linear regression model (or $\mathrm{FAP_{lin}} < 10^{-4}$) are classified as linear *(+)*, if the source brightens over time, or linear *(−)* if the source becomes fainter with time. The remaining YSOs are further classified into secular (periodic, curved) or stochastic (burst, drop, irregular) variables according to a selection of criteria defined by W. Park et al. (2021).

The aim to identify long-term FUor outbursts already discards the light curves falling into a classification as stochastic or periodic ($P < 1400$ days). An inspection of Figure 7 in W. Park et al. (2021) shows that the *linear (−)* and linear *(+)* categories identified in that work are an ideal place to search for the slow-rising outbursts and those that show continuous dimming after reaching peak brightness. YSOs classified as curved could contain some outbursts, but are likely of an intermediate duration. Previous experience in the analysis of mid-IR light curves shows that YSOs that are well fitted by a sinusoidal curve with long periods ($P \geqslant 3000$ days) already fall in the linear category defined in W. Park et al. (2021).

We searched for objects that fall in the *linear* classification of W. Park et al. (2021) by analyzing the mid-IR light curves of the 99,702 SPICY objects. First, we selected YSOs with at least 12 epochs in both W1 and W2. The latter condition is fulfilled by 45,636 YSOs (or 46% of the sample). From these, 37,847 YSOs, or 38% of the sample, fulfill either $\Delta_{W1}/\sigma_{W1} \geqslant 3$ or $\Delta_{W2}/\sigma_{W2} \geqslant 3$. Finally, we find 1087 and 2043 *linear* YSOs in W1 and W2, respectively.

We also explored the available data at near-IR (K_s) wavelengths. However, we are unable to use exactly the same methods as W. Park et al. (2021) to classify the light curves at these wavelengths. Using the same threshold for the FAPs as W. Park et al. (2021) yields almost every variable candidate being classified as *linear*. The higher cadence of VVV observations may lead to this problem, as discussed below.

The FAPs are defined following R. V. Baluev (2008), as

$$\mathrm{FAP}_A = (1 - P_A)^{((N_{\mathrm{epochs}} - D_A)/2)}, \tag{2}$$

with D_A as the number of parameters in the model and P_A as the statistical power of the best-fit "A" hypothesis, defined as

$$P_A = \frac{\chi_N^2 - \chi_A^2}{\chi_N^2}, \tag{3}$$

with χ_N^2 and χ_A^2 as the chi-squared values of the nonvarying and "A" hypothesis, respectively. The values of the FAPs decrease with increasing numbers in degrees of freedom (or increasing epochs of observations). Due to this dependence and the larger number of epochs in VVV observations, $\mathrm{FAP_{lin}}$ and $\mathrm{FAP_{LSP}}$ become too low and reach almost zero, leading to almost every variable candidate being classified as *linear* in the near-IR.

Objects that are classified as *linear* or *periodic* from their mid-IR WISE data show values of the statistical power P_A, defined above, that are above $P_A \sim 0.7$.

For the VIRAC2 near-IR light curves, we calculate P_A for the best-fit linear ($P_{A,\mathrm{lin}}$) and periodic ($P_{A,\mathrm{LSP}}$) models. From a visual inspection of light curves with $P_A > 0.7$, we determine that objects with values above this threshold are well fitted by linear or periodic models. Then, the classification for optical and near-IR light curves that show $\Delta/\sigma \geqslant 3$ follows the criteria

$$\begin{array}{llll} \text{linear} & P_{A,\mathrm{lin}} \geqslant 0.7 & & \\ \text{periodic} & P_{A,\mathrm{lin}} < 0.7 & P_{A,\mathrm{LSP}} \geqslant 0.7 & P < 1400 \quad \text{days} \\ \text{curved} & P_{A,\mathrm{lin}} < 0.7 & P_{A,\mathrm{LSP}} \geqslant 0.7 & P \geqslant 1400 \quad \text{days}, \end{array}$$

with the remaining YSOs with $\Delta/\sigma \geqslant 3$ being classified into the different stochastic classes following the same criteria as W. Park et al. (2021).

From the group of candidate variable YSOs, 717 (0.72% of the sample) are well fitted by a linear model in both W1 and W2, and are therefore classified as *linear*. From these, 526 have negative slopes (linear *(−)*), while 191 show positive slopes (linear *(+)*). From the 717 *linear* objects identified from mid-IR data, 235 have near-IR data from the VVV survey. We find that 86 of them are also classified as *linear* from the 2010–2019 K_s data. From 191 linear *(+)* YSOs, 28 have the same classification from their VVV light curves. In the case of 526 linear *(−)* objects, 57 are classified as linear *(−)* in K_s. Only in one object, we find a classification as linear *(−)* in the mid-IR while having a linear *(+)* in the near-IR (SPICY 43479). Although the different classification may arise from noncontemporaneous coverage between WISE/NEOWISE and VVV, we cannot discard that the anticorrelation could be associated with structural changes of the inner accretion disk (G. R. Bryan et al. 2019).

The variability parameters and classification for the mid-IR light curves of 717 *linear* YSOs are presented in Table 1. The same parameters arising from near-IR light curves are also presented, when available.

[15] Δ is defined as the maximum–minimum magnitude, and σ is calculated by adding, in quadrature, the mean error and the standard deviation (in magnitudes) of the exposures in each epoch.

Table 1
Information on the 717 SPICY YSOs Classified as *Linear* from Their Mid-IR Light Curves

SPICY ID	R.A. (J2000)	Decl. (J2000)	YSO Class	I1	I1err	I2	I2err	W1	W1err	W2	W2err	K_s	$K_s$err	ΔW1	ΔW2	ΔK_s	N_{W1}	N_{W2}	N_{Ks}	Var Class ($W1$,$W2$)	Var Class (K_s)
11492	11:43:09.5	−62:21:13.3	Class II	13.40	0.07	12.42	0.11	11.78	0.82	10.75	0.76	15.08	0.06	2.37	2.30	4.32	16	16	126	linear (+)	irregular
15180	12:57:44.2	−62:15:06.4	FS	12.27	0.04	10.98	0.05	10.37	0.60	9.23	0.46	12.98	0.02	2.23	1.70	2.47	18	18	158	linear (+)	linear (+)
15470	13:01:20.7	−62:20:01.6	Class II	9.55	0.04	8.65	0.04	9.89	0.15	8.72	0.12	11.86	0.02	0.52	0.46	0.60	18	18	149	linear (−)	linear (−)
21349	14:12:48.7	−61:22:50.6	Class II	8.97	0.03	8.24	0.04	9.48	0.24	8.40	0.25	11.12	0.02	0.80	0.85	0.48	17	17	111	linear (−)	irregular
29017	15:45:18.4	−54:10:36.9	Class II	12.16	0.07	11.40	0.07	9.57	0.43	8.70	0.41	11.70	0.02	1.97	1.88	2.83	17	17	133	linear (+)	linear (−)
31759	15:59:26.3	−51:57:11.5	Class II	13.36	0.09	12.35	0.11	10.31	0.29	9.16	0.33	12.52	0.03	0.90	0.86	4.33	14	14	360	linear (−)	irregular
35235	16:18:24.8	−48:54:32.1	Class II	9.91	0.06	9.23	0.05	10.36	0.21	9.36	0.21	11.66	0.02	0.71	0.68	0.46	17	17	124	linear (−)	linear (−)
36590	16:23:27.1	−49:44:43.6	FS	12.56	0.07	11.36	0.07	11.02	0.31	9.76	0.31	13.67	0.03	1.08	1.12	3.80	14	14	123	linear (−)	curved
42901	16:51:57.8	−45:42:39.3	FS	9.27	0.04	8.29	0.04	9.18	0.11	8.18	0.19	11.58	0.02	0.42	0.64	0.93	17	17	191	linear (−)	irregular
57130	17:34:23.1	−30:52:23.3	Class II	8.76	0.05	7.67	0.04	9.26	0.17	7.85	0.15	11.81	0.02	0.54	0.45	0.68	17	17	189	linear (−)	linear (−)
63130	17:46:33.8	−29:22:44.9	Class I	10.79	0.05	8.95	0.04	9.86	0.59	7.87	0.28	14.93	0.06	2.07	0.94	4.54	17	17	225	linear (+)	irregular
65417	17:48:26.3	−24:07:33.2	Class II	8.93	0.04	8.15	0.03	9.66	0.18	8.55	0.19	11.20	0.03	0.74	0.75	0.83	17	17	289	linear (−)	linear (−)
68600	17:55:01.0	−28:01:27.4	Class II	9.31	0.04	8.43	0.04	9.49	0.16	8.38	0.15	11.32	0.03	0.57	0.48	0.96	17	17	196	linear (−)	linear (−)
68696	17:55:15.3	−28:52:58.3	Class II	9.01	0.02	8.22	0.03	9.64	0.13	8.46	0.11	11.74	0.02	0.48	0.46	0.62	17	17	191	linear (−)	linear (−)
87984	18:36:46.3	−01:10:29.5	Class I	8.73	0.03	8.01	0.05	9.17	0.18	8.00	0.20	⋯	⋯	0.51	0.60	⋯	17	17	⋯	linear (−)	⋯
95397	18:57:20.3	+01:57:12.2	Class II	11.48	0.04	10.55	0.05	7.68	0.79	6.80	0.69	⋯	⋯	3.55	3.24	⋯	16	16	⋯	linear (+)	⋯
99341	19:11:38.8	+09:02:59.1	Class II	12.67	0.06	11.73	0.07	9.38	0.70	8.43	0.65	⋯	⋯	3.03	2.84	⋯	16	16	⋯	linear (+)	⋯
100587	19:17:17.9	+11:16:32.3	Class II	11.12	0.05	10.44	0.06	11.44	0.43	10.52	0.46	⋯	⋯	1.34	1.50	⋯	16	16	⋯	linear (−)	⋯
109102	20:23:57.1	+38:51:39.7	FS	11.09	0.03	10.37	0.03	11.30	0.02	10.37	0.03	⋯	⋯	0.11	0.13	⋯	17	17	⋯	linear (−)	⋯
111302	20:30:55.7	+38:40:23.1	Class II	9.14	0.03	8.55	0.04	8.96	0.15	8.21	0.18	⋯	⋯	0.48	0.56	⋯	17	17	⋯	linear (−)	⋯

Note. The displayed version only contains the 20 YSOs with spectroscopic data that are discussed in the main text.

(This table is available in its entirety in machine-readable form in the online article.)

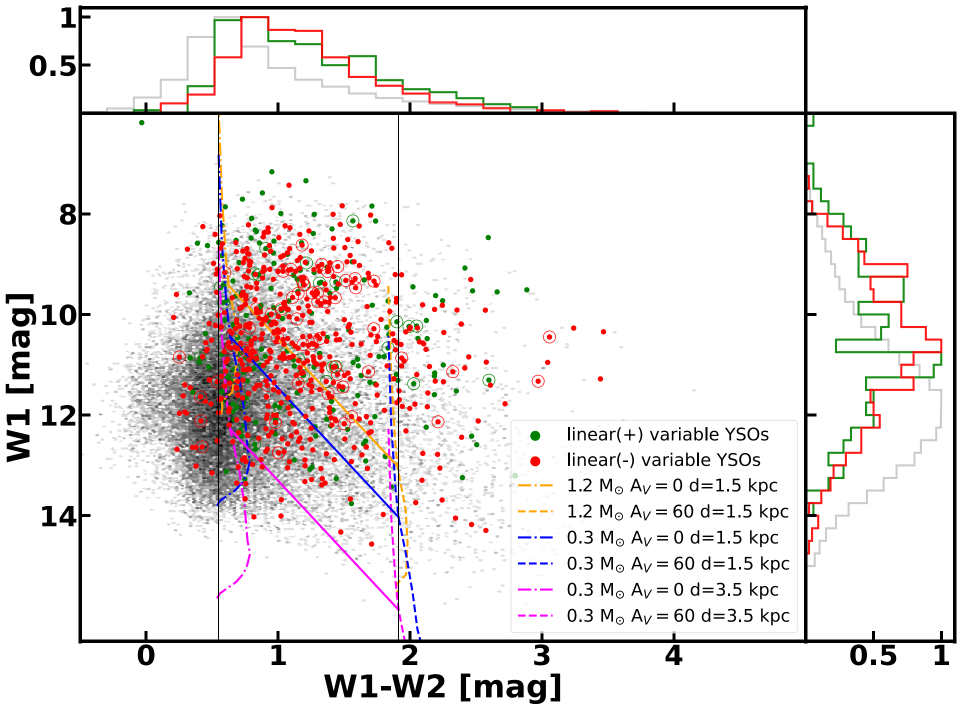

Figure 2. W1 vs. W1 − W2 CMD for SPICY YSOs (gray symbols). YSOs that are classified as linear (−) from their mid-IR light curves are shown as red filled circles, while linear (+) YSOs are shown in green filled circles. YSOs that have near-IR light curves with linear (+) or linear (−) classification are marked by red and green open circles, respectively. Isomass curves for an FUor outburst, as the mass accretion rate increases, are shown for a YSO with mass of the central star of $M = 0.3M_\odot$ and $M = 1.2M_\odot$. The curves, taken from H. Liu et al. (2022), are artificially set at distances of 1.5 and 3.5 kpc and are shown for $A_V = 0$ and $A_V = 60$ mag. The blue, pink, and orange solid lines connecting the curves mark the point where the disk dominates emission. The vertical black solid lines roughly mark the colors of systems with $A_V = 0$ and 60 mag from the H. Liu et al. (2022) models.

3.1. Candidate FUors

In Figure 2, we show the W1 versus W1 − W2 color–magnitude diagram (CMD) for SPICY YSOs with available WISE photometry, as well as the location of 717 YSOs classified as *linear*. In the same figure, we also show the location of FUor outbursts in the CMD, as predicted by the SED models of FUor outbursts from H. Liu et al. (2022). We compare with models for a mass of the central star of $M_\star = 0.3\,M_\odot$ and $M_\star = 1.2\,M_\odot$. The magnitudes and colors are corrected for distances of 1.5 and 3.5 kpc, and extinction values in the V band of $A_V = 0$ and $A_V = 60$ mag. The extinction at the wavelengths of the WISE filters is estimated using the K. D. Gordon et al. (2021) Milky Way extinction curves. In the figure, we also mark the point in the isomass tracks of FUor outbursts at which the disk dominates the emission from the YSO. We find that FUors can be located over a wide range of magnitudes, depending on the distance to the source. The colors of these systems, however, are mostly contained in the region $0.55 < \mathrm{W1} - \mathrm{W2} < 1.91$ mag.

Figure 2 shows that the distribution of W1 − W2 color of *linear* sources appears to peak at redder values compared with the distribution for the overall sample of SPICY objects. We find that 92% of the *linear* YSOs are located at $\mathrm{W1} - \mathrm{W2} > 0.55$ mag (the lower limit defined by the H. Liu et al. 2022 models). If we take $\mathrm{W1} - \mathrm{W2} \simeq 1.91$ mag, the color defined by H. Liu et al. (2022) models with $A_V = 60$ mag (close to the maximum value of A_V for known FUors in M. S. Connelley & B. Reipurth 2018), as an upper limit to define the region where FUors are preferentially located, we find that 82% of *linear* objects are in this region. The *linear* sources are also located at brighter magnitudes compared with the overall sample of protostars, which would agree with the expectations of these objects being candidate FUors. However, we cannot discard the possibility that this is associated with our inability to classify fainter sources with larger uncertainties in magnitude. Similar distributions and conclusions are derived when only considering the objects that have a *linear* classification from VVV data.

Differences also exist among the YSOs classified as *linear*. In Figure 3, we show the absolute value of the average change in magnitude per year versus the W1 − W2 color for the *linear* YSOs. Here, we find that the majority of the sources show shallow slopes, with changes in most sources (∼90%) located at values lower than 0.1 mag yr^{-1}. The visual inspection of Figure 3 seems to indicate that linear (+) YSOs have a distribution that is slightly skewed toward bluer W1 − W2 colors and a slightly higher fraction of objects with larger values of the slope. We evaluate these statements by performing a set of different statistical tests (Kolmogorov–Smirnov, Wilcoxon, and Anderson–Darling) on these distributions. The tests support the differences in color distribution between the two samples (although with some dependence on the chosen bin size). However, we cannot conclude that the two samples show differences in the distribution of the slope.

The validity of any analysis based on the sample defined above depends on whether all objects in our *linear* sample are FUor outbursts. Confirming this requires an analysis of the expected degree of contamination as well as a spectroscopic follow-up of our sample.

3.2. Contamination

The photometric characteristics of the *linear* sources, discussed in the previous section, are in line with the expectations of FUors and can therefore be classified as

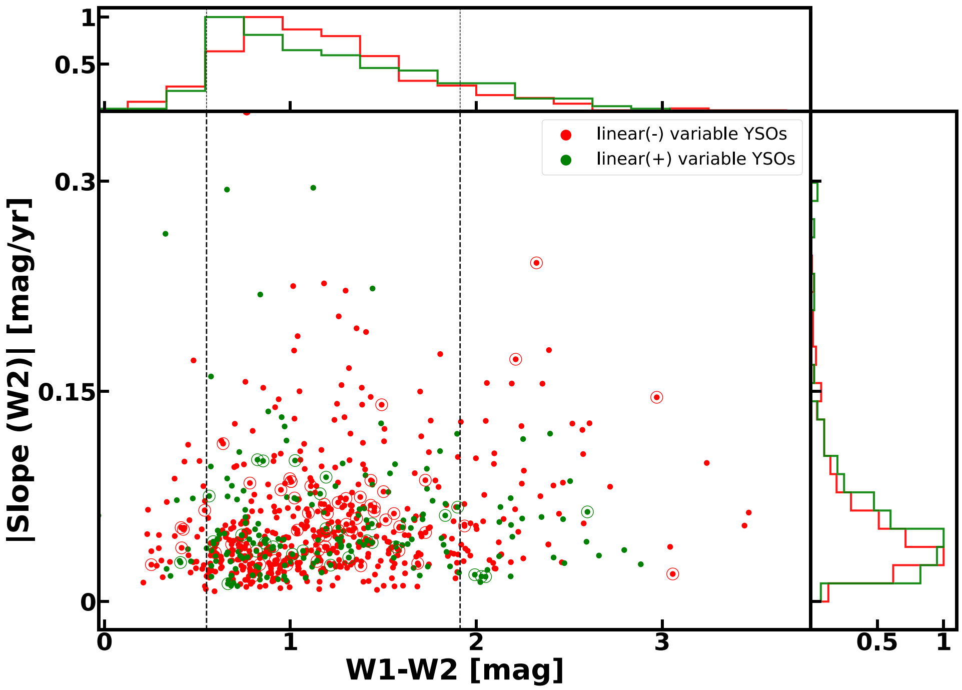

Figure 3. Average change per year (in magnitudes) vs. W1 − W2 color for YSOs that are classified as *linear*. The vertical black solid lines roughly mark the colors of systems with $A_V = 0$ and 60 mag from the H. Liu et al. (2022) models. Symbols are the same as in Figure 2.

candidate FUors. However, we also need to consider the possibility of other classes of variable stars contaminating our sample (see, e.g., J.-E. Lee et al. 2021b).

M. A. Kuhn et al. (2021) discuss the possibility of evolved stars, such as asymptotic giant branch (AGB) stars, and extragalactic sources as the two main sources of contamination in their sample. Both types of objects can mimic the near- to mid-IR colors of YSOs and therefore contaminate YSO searches (see, e.g., T. P. Robitaille et al. 2008). The evolved sources can also complicate the interpretation of the long-term declines in our sample. Some symbiotic stars show similar long-term declines in their optical light curves (see, e.g., Figure 1 in M. Gromadzki et al. 2009).

M. A. Kuhn et al. (2021) expect a low level of contamination, as evolved and extragalactic sources tend to be located in areas that are flagged as contaminants in their analysis, and therefore are less likely to be included in the SPICY catalog. Z. Guo et al. (2022) find 253 SPICY sources that show periodic light curves that are likely associated with pulsation in evolved stars. Meanwhile, M. A. Kuhn et al. (2023) spectroscopically assessed the contamination to be <10% for the subset of optically bright SPICY sources. However, there is no formal assessment of contamination by M. A. Kuhn et al. (2021), as this would require a more complete spectroscopic follow-up.

FUors are identified due to their unique spectroscopic characteristics during an outburst. These include the gradual change of spectral type with wavelength, a lack of emission lines, and absorption from water vapor and other molecular bands, including the appearance of strong and broad ^{12}CO $\nu = 2$–0 absorption at 2.2935 μm (M. S. Connelley & T. P. Greene 2010; M. S. Connelley & B. Reipurth 2018). During the outburst, the accretion disk dominates emission in the system, where absorption lines arise due to a cooler disk surface compared with the viscously heated midplane (G. H. Herbig 1977; L. Hartmann & S. J. Kenyon 1996; H. Liu et al. 2022).

The near-IR spectroscopic characteristics of FUors are very similar to those of K–M giant stars. In addition, the FUor spectra can, broadly speaking, resemble the mid to late M-type atmospheres of young brown dwarfs (e.g., M. S. Connelley & B. Reipurth 2018). For the latter, we argue that, given the typical distances of the SPICY sample and the low luminosities of brown dwarfs, these objects would be located toward the faint magnitude limits of the WISE observations. Therefore, it is unlikely that objects in our candidate FUors sample are brown dwarfs.

In the case of evolved stars, we can use additional evidence to discard contamination from these sources. For example, the observation of ^{13}CO absorption is a useful indicator of the evolved nature of a source (C. Contreras Peña et al. 2017b; Z. Guo et al. 2021). In addition, field giant stars show low rotation velocities, which would not lead to broadened absorption features. Only 2% of giant stars investigated by J. K. Carlberg et al. (2011) show a projected rotational velocity, $v \sin i$, larger than 10 km s^{-1}; this fraction reduces to 0.7% of the sample for $v \sin i > 20$ km s^{-1}. However, giant stars in symbiotic systems show faster rotation than field giant stars, with some evolved objects in D-type symbiotic systems showing rotation with $v \sin i \sim 30$–40 km s^{-1}. The infrared colors of these systems, especially D-type symbiotics, overlap with those of YSOs in CMDs used for the classification of objects (see, e.g., R. L. M. Corradi et al. 2008).

High-resolution spectroscopy is useful to determine velocities from rotational or disk broadening (e.g., S. Park et al. 2020) and to discriminate FUors from background giant stars. Using velocities to discriminate becomes more complicated for low-resolution and midresolution spectroscopy.

The issue of potential contamination will be taken into account when analyzing the spectra of 20 candidates in the following sections.

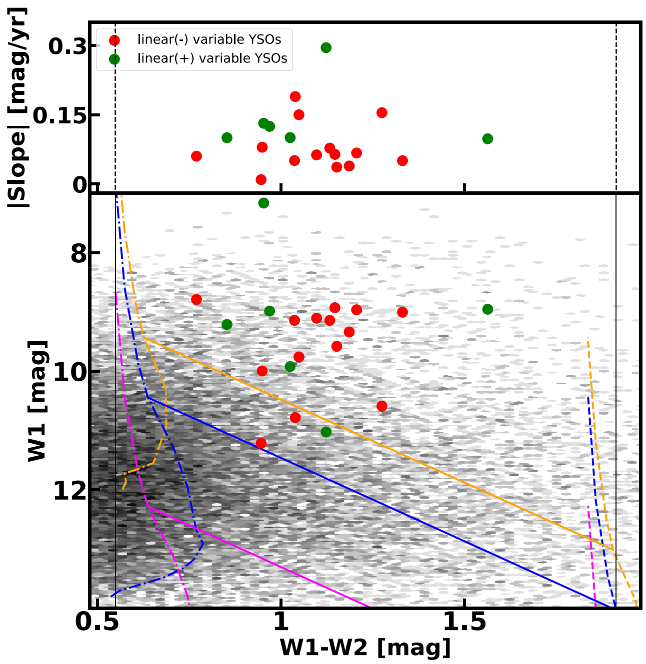

Figure 4. Location in average change per year (in magnitudes) vs. W1 − W2 color (top), and W1 vs. W1 − W2 color–magnitude (bottom) diagram of 20 *linear* YSOs with spectroscopic data. Gray symbols and overlaid lines are the same as in Figure 2.

4. Follow-up of Candidate FUors

From the list of candidate FUors, we carried out a spectroscopic follow-up of 10 sources that were bright enough to obtain moderate-to-high signal-to-noise ratio observations with the Gemini/Immersion Grating Infrared Spectrometer (IGRINS) and Infrared Telescope Facility (IRTF)/Spex instruments. We were also able to find spectroscopic information in the literature for 10 additional sources. Information on the distance and evolutionary stage for the 20 sources is presented in Table 3 and the Appendix.

The locations of the 20 sources in the CMD and the slope-versus-color diagram are shown in Figure 4. We observe that the majority of sources are located within the regions defined by the H. Liu et al. (2022) theoretical models of FUor outbursts using extinction values of $A_V = 0$ and 60 mag (marked by the black lines in the figure). Most sources show shallow values of the slope in Figure 4, with linear $(-)$ objects tending to locate at lower values than objects classified as linear $(+)$.

4.1. Spectroscopy from the Literature

In 10 objects, we find near-IR spectroscopic data in the literature. These include IRTF/SpeX observations of SPICY 87984 (M. S. Connelley & T. P. Greene 2010), 95397, 99341, and 100587 (C. Contreras Peña et al. 2023a). In addition, we find ESO Very Large Telescope/X-shooter observations for SPICY 11492, 31759, and 63130 (Z. Guo et al. 2024a). Finally, Magellan/FIRE observations of SPICY 15180, 29017, and 36590 were published by C. Contreras Peña et al. (2017a) and Z. Guo et al. (2021).

4.2. IRTF/SpeX Spectroscopy

We obtained near-IR spectra of SPICY 109102 and 111302 on 2023 October 7 and 8 (Hubble Space Telescope) using SpeX (J. T. Rayner et al. 2003) mounted at the NASA IRTF on Maunakea (program 2023B079, PI: Contreras Peña). The cross-dispersed spectra cover 0.7–2.5 μm spectra at $R \sim 2000$, obtained with the 0.5″ slit. Total integration times ranged from 480 to 840 s, with individual exposures of 60 s. Bright A0V standard stars were observed for telluric calibration. All spectra were reduced and calibrated using Spextool version 4.1 (M. C. Cushing et al. 2004).

Table 2
Information on the Eight SPICY YSOs with IGRINS Observations

SPICY ID	Standard	Obs Date	Exp Time (s)
SPICY 15470	HIP 58898	2023 Feb 19	8 × 360
SPICY 21349	HIP 83066	2023 Mar 15	8 × 310
SPICY 35235	HIP 79477	2023 Mar 15	8 × 360
SPICY 42901	HIP 84267	2023 Mar 18	8 × 340
SPICY 57130	HIP 86098	2023 Mar 16	8 × 360
SPICY 65417	HIP 79332	2023 Feb 19	8 × 320
SPICY 68600	HIP 85871	2023 Mar 17	8 × 340
SPICY 68696	HIP 83399	2023 Mar 17	8 × 360

4.3. Gemini South/IGRINS Spectroscopy

We observed eight YSOs that were selected as candidate FUors with IGRINS installed at the 8.1 m Gemini South telescope between 2023 February 18 and 2023 March 17 (program GS-2023A-Q-207; PI: Lee, H.-G.). IGRINS simultaneously covers the H (1.49–1.80 μm) and K (1.96–2.46 μm) bands, with $R \simeq 45{,}000$ (G. Mace et al. 2018).

The observations were carried out on an ABBAABBA pattern, with individual exposure times between 310 and 360 s. The spectra have been reduced by the IGRINS pipeline.[16] Standard A0 stars were observed immediately after the observation of each FUor candidate for purposes of telluric correction. The dates of observations and the standard star used for correction are presented in Table 2.

4.4. Historical Light Curves

For the 20 sources with spectroscopic data, we collected additional photometry from optical, near-, and mid-IR surveys available through the VizieR catalog access tool (F. Ochsenbein et al. 2000). For most cases, the oldest available data arise from the 2MASS or DENIS (N. Epchtein et al. 1994) surveys.

In three objects, SPICY 29017 (linear $(+)$), 65417 (linear $(-)$), and 99341 (linear $(+)$), we have optical photometry from Gaia. For these objects, we searched digitized photographic plate images from the SuperCOSMOS survey (N. C. Hambly et al. 2001). In SPICY 65417, the oldest photographic plate images were taken in 1985. A comparison with the PanSTARRS r-band cutout image shows that the star was at a similar brightness level. This implies that, if this is truly an FUor, the object went into an outburst more than 38 yr ago. In SPICY 99341, the photographic plate images were taken between 1950 and 1995, and in none of them can we see the source. PanSTARRS r- and i-band cutout images confirm the outburst of the source around 2010–2011. A similar date for the outburst is reached when comparing WISE and UKIDSS data (C. Contreras Peña et al. 2023a). Finally, SPICY 29017 does not show up in the photographic plate images (1977–1991 observations). There is a faint source at the

[16] https://github.com/igrins/plp

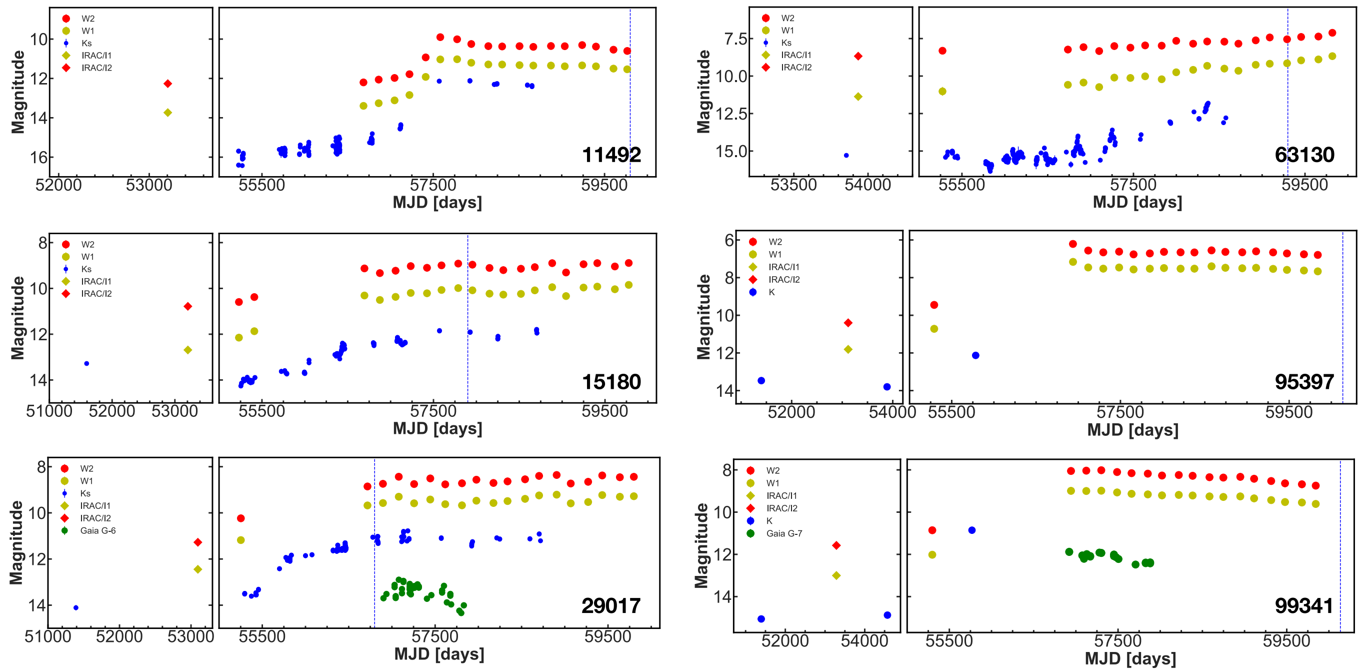

Figure 5. Gaia G (green), near-IR K/K_s (blue), mid-IR W1/IRAC1 (yellow), and W2/IRAC2 (red) light curves of six linear (+) YSOs with spectroscopic data. The blue vertical line marks the date of the spectroscopic follow-up.

location of SPICY 29017 that shows up in *r*- and *i*-band images from the SkyMapper Southern Survey (C. A. Onken et al. 2019) taken at similar dates to the Gaia observations, which would point to a recent outburst of the source. The source is brighter in *z*-band images from Skymapper, but the images taken in 2016 and 2017 show a decline in brightness, which agrees with the Gaia light curve. The light curves of these 6 linear (+) and 14 linear (−) objects with spectroscopic data are shown in Figures 5 and 6, respectively.

5. Spectroscopic Confirmation of Linear FUors

5.1. Objects in the Literature

Linear (−). SPICY 87984 (IRAS 18341−0113N) is part of the Class I sample of M. S. Connelley & T. P. Greene (2010). In their work, the near-IR spectrum of the source shows a triangular *H*-band continuum, ^{12}CO absorption, which is in excess for the best-fit spectral type for the YSO (K0-M4), and a lack of emission lines. Given some of the similarities to FUor spectra, M. S. Connelley & T. P. Greene (2010) note that this object might be experiencing weak FUor-like activity.

SPICY 31759 (L222_33, Z. Guo et al. 2024a), SPICY 36590 (VVVv270, C. Contreras Peña et al. 2017b, 2017a), and SPICY 100587 (C. Contreras Peña et al. 2023a) all show high-amplitude outbursts ($\Delta K_s > 2.5$ mag). The outbursts occurred prior to the coverage of WISE/NEOWISE, which explains their classification as linear (−) sources. The spectra of YSOs SPICY 31759 and 100587 show similarities to those of classical FUors and are therefore classified as this type of outburst (see C. Contreras Peña et al. 2023a; Z. Guo et al. 2024a). The spectrum of SPICY 36590, taken close to the maximum point in the light curve, shows ^{12}CO emission in spite of the high amplitude and long duration of the outburst. The magnetospheric accretion process might still be in control in this type of eruptive variable YSO (Z. Guo et al. 2021; and Section 5.4).

Linear (+). SPICY 11492 (L222_1), 63130 (L222_148), 15180 (Stim 1), and 29017 (VVVv631) are all part of previous publications from the VVV team (C. Contreras Peña et al. 2017a; Z. Guo et al. 2021, 2024a; P. W. Lucas et al. 2024). The four sources show long-term rises in their light curves, both at near- and mid-IR wavelengths. These long-term trends were noticed by Z. Guo et al. (2024a), with SPICY 63130 also showing quasiperiodic ($P \sim 378$ day) variability on top of the long-term rise. Only in SPICY 11492, the spectrum resembles that of classical FUors with strong ^{12}CO absorption at near-IR wavelengths. SPICY 63130 and 15180 both show emission line spectra. Finally, SPICY 29017 shows ^{12}CO emission and H_2O absorption. This combination, which has also been observed in the eruptive YSO V1647 Ori, could be explained by a hot inner disk, which generates the ^{12}CO emission, and where water absorption is generated in a cooler location farther out in the disk (Z. Guo et al. 2020).

SPICY 99341 and 95397 are both classified as linear (+); however, due to the gap between WISE and NEOWISE observations, we cannot claim that these are examples of slow-rising outbursts. SPICY 99341 is source #266 of the UKIDSS GPS high-amplitude variable star sample (P. W. Lucas et al. 2017) as it shows $\Delta K \simeq 4$ mag. The spectroscopic follow-up of the YSO yields an FUor classification (C. Contreras Peña et al. 2023a). SPICY 95397 has previously been classified as a mid-IR high-amplitude star (source #21, P. W. Lucas et al. 2020), but its spectrum shows strong ^{13}CO absorption. The strength of these rovibrational bands depends on the abundance of ^{13}C (J. Poorta et al. 2023). Therefore, these absorption bands are commonly found in the spectra of evolved stars, where chemical enrichment has led to $^{12}C/^{13}C$

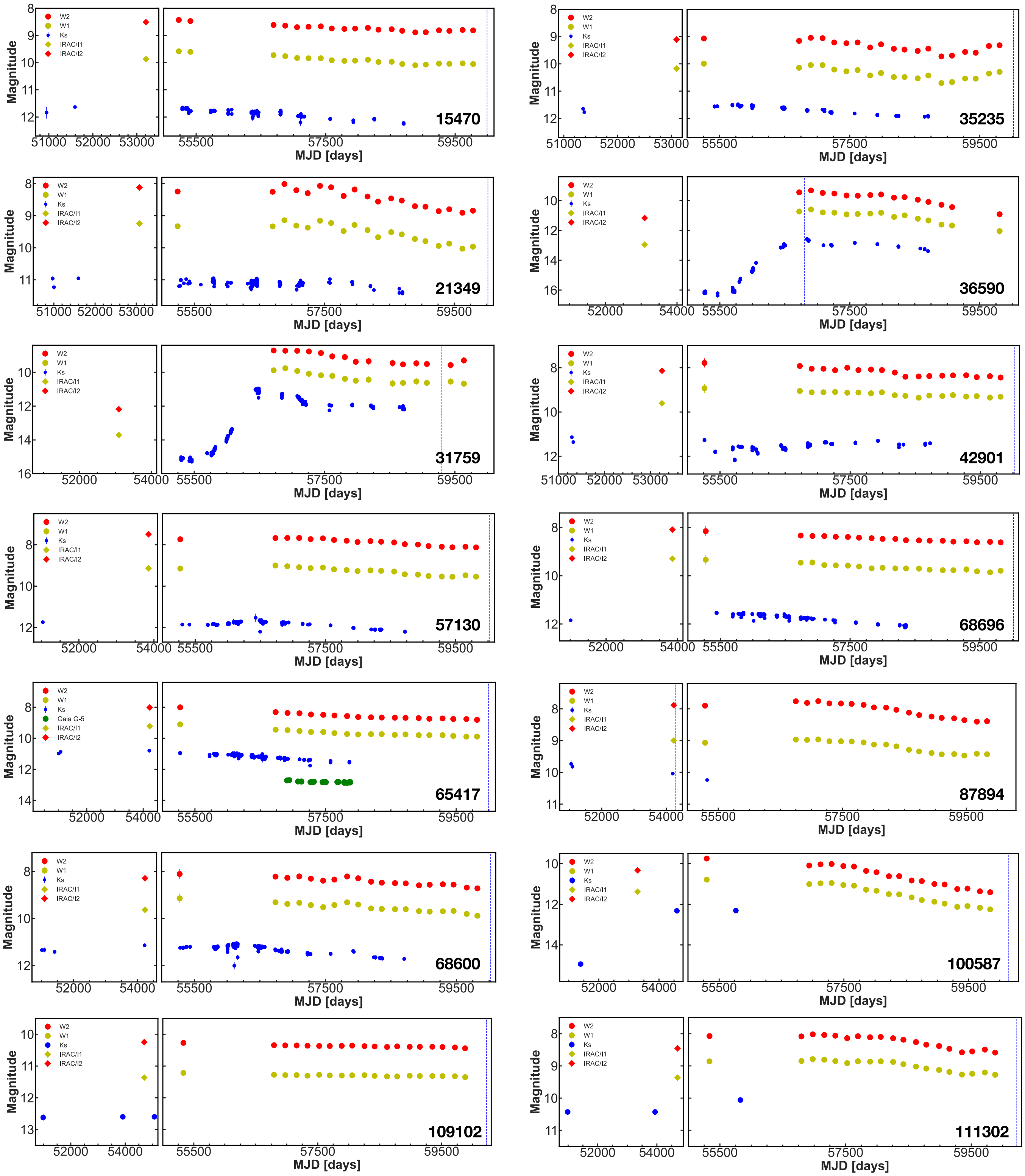

Figure 6. Near-IR K/K_s (blue), mid-IR W1/IRAC1 (yellow), and W2/IRAC2 (red) light curves of 14 linear (−) YSOs with spectroscopic data. The blue vertical line marks the date of the spectroscopic follow-up.

ratios of <30 (see, e.g., K. H. Hinkle et al. 2019). These ratios are lower than the one found in the interstellar medium, and also expected in YSOs, of $^{12}C/^{13}C \sim 89$ (J. Poorta et al. 2023).

Given the observed ^{13}CO features, SPICY 95397 is classified as a contaminating evolved source by C. Contreras Peña et al. (2023a).

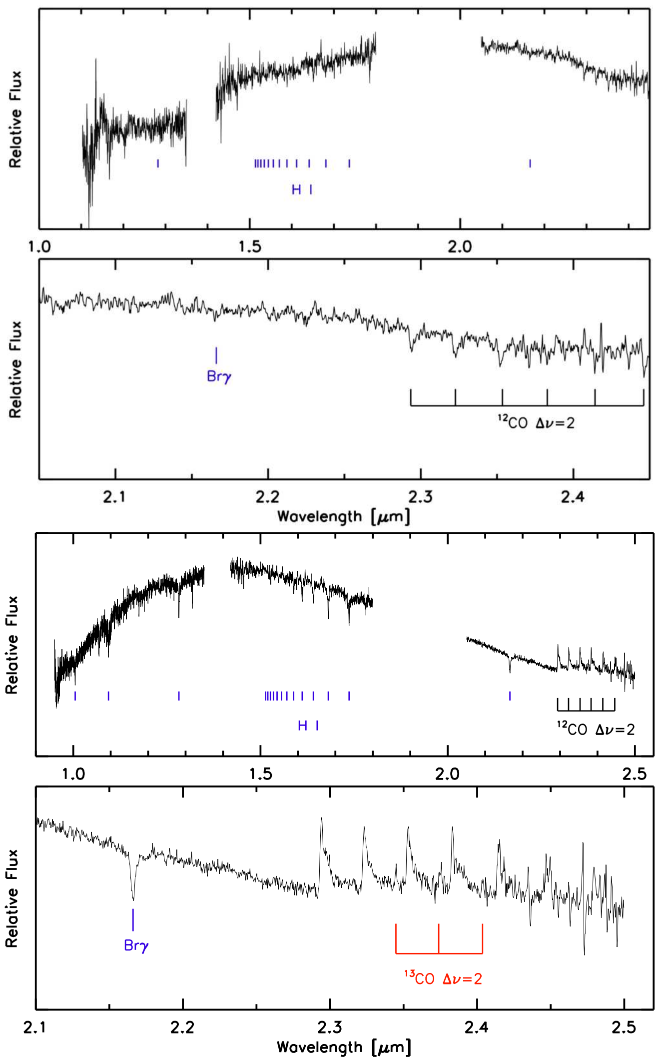

Figure 7. Near-IR spectra of SPICY 109102 (top two panels) and SPICY 111302 (bottom two panels). The location of H I lines from the Paschen and Brackett series, as well as from ^{12}CO $\nu = 2$–0 rovibrational transitions, are marked in both figures. For SPICY 111302, we also mark the location of ^{13}CO $\nu = 2$–0 rovibrational transition lines.

5.2. New Objects from IRTF/SpeX

SPICY 109102 and 111302 are both classified as linear ($-$) based on their WISE/NEOWISE light curves. The long-term behavior is confirmed by Spitzer and 2MASS observations. The near-IR IRTF/SpeX spectra of both sources are shown in Figure 7.

The near-IR spectrum of SPICY 111302 shows strong ^{12}CO emission as well as absorption from several hydrogen recombination lines (see Figure 7). ^{12}CO emission is generally observed in eruptive YSOs classified as EX Lupi–type (e.g., D. Lorenzetti et al. 2012; and Section 5.4). The presence of ^{13}CO $\Delta\nu = 2$ bandhead emission, however, is a strong indicator of chemical enrichment, and has been observed in the spectra of evolved stars (M. E. Oksala et al. 2012; M. Kraus et al. 2020; Y. R. Cochetti et al. 2021; J. Poorta et al. 2023). The ^{13}CO emission and strong H I absorption are not a feature (to the best of our knowledge) of EX Lupi–type objects. In addition, the lack of Na I emission is not common in the latter class of eruptive YSOs. The features are more likely to arise from a decretion disk, indicating that SPICY 111302 is an evolved star rather than a YSO.

The spectrum of SPICY 109102 is nearly featureless, except for the presence of strong ^{12}CO absorption beyond 2.29 μm. We cannot detect any Ca I, Na I, or water vapor absorption. The strength of ^{12}CO compared with Na I + Ca I would be in line with an FUor classification (M. S. Connelley & B. Reipurth 2018). However, the lack of an observed outburst would only allow for an FUor-like classification of the source.

5.3. High-resolution IGRINS Spectra: FUor-like Sources

Figure 8 shows the ^{12}CO $\nu = 2$–0 region of the spectra for six candidate FUors with IGRINS observations. Their spectra show strong and broad ^{12}CO absorption that resembles that of the known FUors V1515 Cyg and FU Ori. In FUor outbursts, line broadening occurs due to disk rotation. V1515 Cyg is the classical FUor with the least broadened ^{12}CO absorption profile, which is attributed to the lower inclination of the system, as compared with, e.g., FU Ori (L. A. Hillenbrand et al. 2019a; Z. M. Szabó et al. 2022). We note that the IGRINS spectra of SPICY YSOs 15470 and 57130 look very similar to that of V1515 Cyg, which could be evidence of low disk inclinations in these systems.

The spectra around the Na I absorption lines provide more evidence that the near-IR spectra of our sample arise from a disk. The six objects show absorption from Na I (Figure 8). These features are not so evident in SPICY 35235, likely due to them being strongly broadened, similar to the spectrum of FU Ori itself. In five out of six objects (Figure 8), we observe absorption from Sc I lines at 22057 and 22071 Å, and for two objects (SPICY 15470 and SPICY 57130), we observe absorption from V I at 22097 Å. A comparison with V1515 Cyg shows that Sc I absorption is also present in this classical FUor. The Sc I and V I lines are stronger in the spectra of M-type giant stars, as compared with K-type atmospheres. For example, Y. Takagi et al. (2011) show that the ratio between the Sc I and Na I lines is sensitive to surface gravity, where objects with $\log g < 2$ show stronger absorption from Sc I.

To provide further evidence of the disk nature of the absorption, the *H*- and *K*-band absorption of the six candidate FUors is fitted by convolving stellar templates from the IGRINS spectral library (S. Park et al. 2018) using a Keplerian disk profile to account for broadening (see Equation (1) in S.-Y. Yoon et al. 2021). The value of the maximum projected rotation velocity ranges between 7 and 110 km s^{-1}, and a veiling factor, *r*, is also introduced following B. Kidder et al. (2021) and S.-Y. Yoon et al. (2021). We used χ^2 minimization to find the best fit. Following J.-E. Lee et al. (2015) and S. Park et al. (2020), 29 regions in the *H* and *K* band are analyzed, which include absorption from, e.g., Fe I (15340, 15670, and 16490 Å), Al I (16755 Å), Na I (22060 and 22090 Å), Ti I (21789 Å), and ^{12}CO $\nu = 2$–0 (22935 Å).

The analysis of these 29 spectral regions in the *H*- and *K*-band data for the six YSOs shows that G8-M3 templates with $v \sin i$ between 12 and 55 km s^{-1} provide good fits to the spectra (see Figure 9 for example regions in the spectrum of SPICY 35235). The expectation in a Keplerian disk model is that the rotational velocity of the disk decreases with wavelength. This is expected because warmer regions near the protostar rotate faster than cooler outer regions (S.-Y. Yoon et al. 2021). The increase in $v \sin i$ has been observed in FUor disks, being more noticeable when comparing optical to

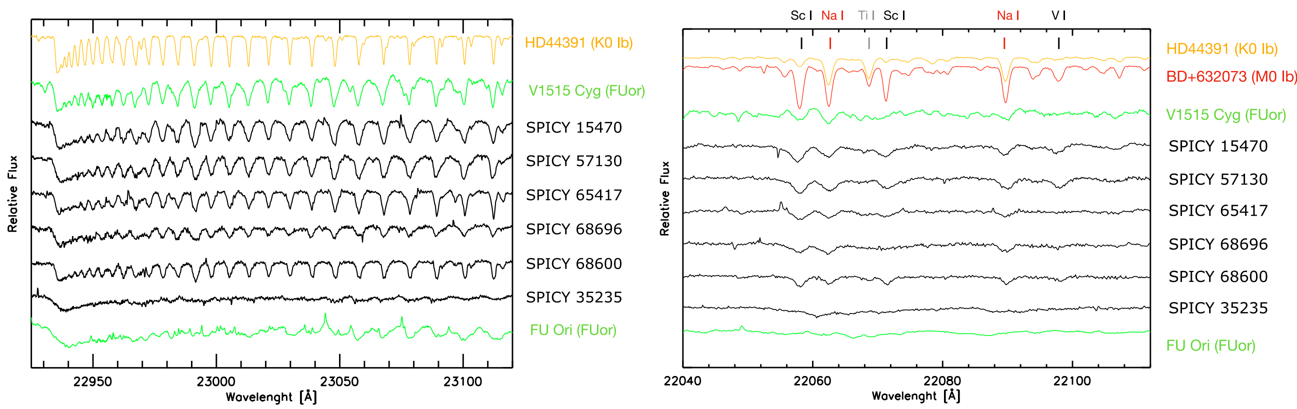

Figure 8. IGRINS spectra of six FUor candidates from our selection (solid black lines). The spectrum is centered around the wavelength of the ^{12}CO $\nu = 2$–0 bandhead absorption.

infrared wavelengths (e.g., Z. Zhu et al. 2007; J.-E. Lee et al. 2015). In four sources, we observe a decrease in the maximum projected rotational velocity as we move toward longer wavelengths, with SPICY 35235 showing the most dramatic change. In two sources, SPICY 15470 and SPICY 68696, the velocities appear to remain constant, and given the lack of optical data, we cannot confirm any decrease toward longer wavelengths. A low value of the inclination in these systems could explain the relatively constant velocities in the 1.5–2.4 μm range.

The lack of an outburst observation in all of these sources still raises some concern regarding possible contamination. In Section 3.2, we have stated that giant stars in D-type symbiotic binary systems show large stellar rotation velocities that could lead to line broadening. These velocities are similar to the ones found for the six sources with IGRINS data. However, R. L. M. Corradi et al. (2008) show that D-type symbiotic stars also have large r-Hα excesses (see their Figure 1). Three of our sources are found in the VPHAS catalog (J. E. Drew et al. 2016). The colors of SPICY 57130 ($r - i = 1.3$, $r - \mathrm{H}\alpha = 0.7$), SPICY 68600 ($r - i = 2.1$, $r - \mathrm{H}\alpha = 0.6$), and SPICY 68696 ($r - i = 2.1$, $r - \mathrm{H}\alpha = 0.6$) are inconsistent with a r-Hα excess and therefore disagree with a D-type symbiotic classification. In addition, our spectra lack the strong H I and He I emission that is commonly observed in symbiotic stars (K. Belczyński et al. 2000).

Therefore, the evidence presented above for the spectral regions in the H and K bands, i.e., broadening consistent with a Keplerian rotation model, favors the accretion disk scenario in our objects.

5.4. High-resolution IGRINS Spectra: Peculiar Outbursts

Two sources, SPICY 21349 and SPICY 42901, show spectra featuring emission in hydrogen Brγ (2.16 μm), Na I (2.26 μm), and ^{12}CO $\Delta\nu = 2$–0 (2.2935 μm) (see Figure 10). These characteristics were usually associated with EX Lupi–type or V1647-Ori–like outbursts, which display outburst durations that are shorter than the typical timescales of FUor outbursts. However, there is growing evidence that long-term outbursts can also display emission line spectra.

The known eruptive YSO SVS13 went into an outburst between 1988 and 1990 and has remained bright ever since, with the spectrum of the object being dominated by emission lines during the outburst (J. Eisloeffel et al. 1991). YSOs VVVv270 and VVVv631 (C. Contreras Peña et al. 2017a) also show long-duration outbursts while displaying emission line spectra during various epochs collected in the bright state (Z. Guo et al. 2020). In fact, the majority of eruptive YSOs that show long-duration outbursts in the sample of Z. Guo et al. (2021) may be controlled by the magnetospheric accretion process, as indicated by the Brγ emission. Therefore, the characteristics of the spectra of SPICY YSOs 21349 and 42091 do not contradict the expectations that these objects are going through long-term outbursts.

To study the ^{12}CO $\nu = 2$–0 emission in both YSOs, we used a similar method as in Section 5.3, but multiplying the stellar templates by -1 to turn the CO features into emission. We find that these features are broadened with $v \sin i = 27$ km s^{-1} and $v \sin i = 39$ km s^{-1} for SPICY 21349 and 42901, respectively, consistent with broadening expected from Keplerian rotation (J. Najita et al. 1996). The strength of the Na I and Brγ emission varies depending on the YSO, with SPICY 21349 showing stronger emission of these spectral features. Several emission lines from the hydrogen Brackett series are also present in the H-band spectra of the source (see Figure 10). Interestingly, the H-band spectrum of SPICY 42901 lacks any further emission from hydrogen lines and is instead dominated by absorption from, e.g., Fe I and Al I (Figure 11). In addition, Sc I is seen as an absorption line at 2.207 μm. These absorption lines appear broader than expected from a stellar photosphere. Some absorption lines also appear broadened in the spectrum of SPICY 21349, but it is less clear in this source. This combination of broad absorption lines and emission lines strengthens the scenario where the flux arises from multiple locations in an accretion disk.

6. On the Timescales and Frequencies of FUor Outbursts

Based on the results from YSOs with spectroscopic data, we find 18 objects that are classified as eruptive variable YSOs, with 9 of these corresponding to new additions to the variable class (7 FUor-like, 2 peculiar). Only two sources are found to be evolved stars (one AGB and one Be star).

Given these results, the method outlined in this work is found to be highly successful in finding eruptive YSOs in the long-term VVV and WISE/NEOWISE data. By assuming that the majority of objects in our sample are true eruptive YSOs, we can provide some insights into the rising and decay timescales of FUor outbursts, as well as reconcile the number of objects in our sample with the estimated frequencies of FUor outbursts.

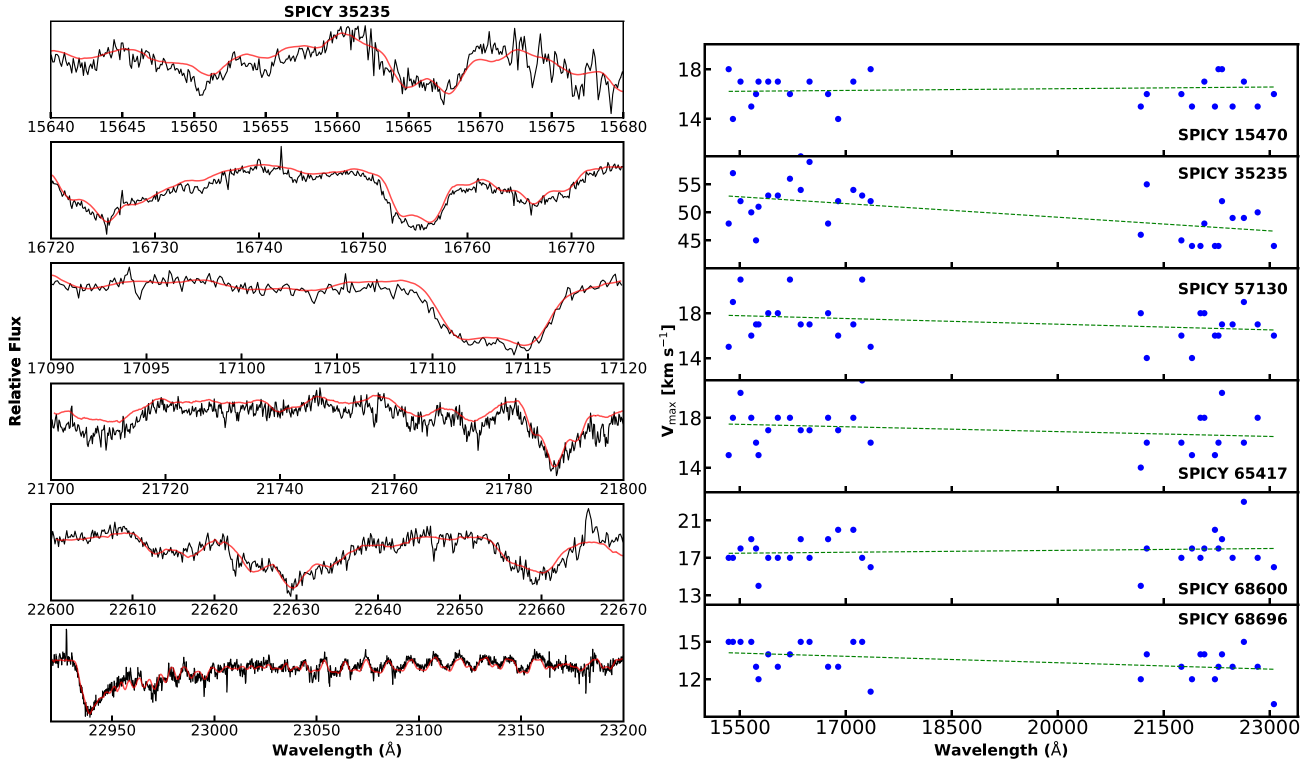

Figure 9. (Left) IGRINS spectra of SPICY 35235 (solid black lines) and the fits using templates from the IGRINS spectral library (red), as described in the main text. (Right) $v \sin i$ vs. wavelength for the 29 regions used to fit the data. The green dashed lines mark linear fits to these data.

6.1. Outburst Timescales

Under the assumption that most of the 717 *linear* YSOs are true eruptive YSOs, the number of sources classified into the linear (−) and linear (+) categories can, tentatively, provide some insight into the rising timescales of FUor outbursts. From the sample of 717 YSOs classified as *linear*, we find a ratio of rising (linear (+)) to fading (linear (−)) objects of 171/526, or ∼0.32.

To quantify the significance of the ratio in terms of rising and decay timescales of outbursts, we constructed a set of synthetic light curves that simulate FUor outbursts. These were built by combining two sigmoid functions, one that simulates the rise and another to simulate the decline of the outburst. The starting time of the latter function is set as the final time of the rise function. The rise timescales, $t_{\rm rise}$ (or the time that it takes to reach 90% of the peak brightness), are set at 100, 300, 500, 800, 1200, 2000, 3500, 5000, and 8000 days. The decay timescales, $t_{\rm decay}$, are set at the same values, but with the condition that $t_{\rm rise} \leqslant t_{\rm decay}$. For all values of $t_{\rm rise}$, we also simulate light curves with $t_{\rm decay}$ = 15,000 and 30,000 days. The amplitudes of the bursts are also varied and are set as Δ = 1.2, 1.6, 2, 2.4, 2.8, and 3.2 mag. The choice of parameters is based on previous observations of FUors. Amplitudes larger than 1 mag are expected in the mid-IR for accretion-driven variability (A. Scholz et al. 2013; A. C. Rodriguez & L. A. Hillenbrand 2022). The rise timescales in the FUors discovered in the VVV survey range between 100 and 2500 days (Z. Guo et al. 2024a). We also allow for longer values of $t_{\rm rise}$ as some of the theoretical mid-IR outbursts by J. Cleaver et al. (2023) can show rises lasting longer than 20 yr, and the mid-IR rising timescales are usually longer than the near-IR timescales, such as in Gaia17bpi (L. A. Hillenbrand et al. 2018) and L222_78 (Z. Guo et al. 2024b). Finally, known FUors show shorter values of $t_{\rm rise}$ compared with the time they spend in the bright state (see, e.g., M. Audard et al. 2014). Examples of simulated light curves are shown in Figure 12.

For given values of $t_{\rm rise}$, $t_{\rm decay}$, and amplitude, we create a synthetic light curve. Then, we follow the steps below:

(a) Select 20 points that follow the observation cadence of WISE/NEOWISE data. The starting point of the observations is selected randomly in the synthetic light curve.
(b) Apply a random measurement error with a maximum value of 0.08 mag.
(c) Classify the new WISE/NEOWISE light curve using the method of Section 3.
(d) Steps (a)–(c) are repeated 2000 times.

We note that ∼20% of the SPICY YSOs are found at either the bright or the faint end of the mid-IR magnitude distribution, and therefore show larger errors (>0.1 mag). To account for the effect of larger errors in the classification process, in ∼20% of the repetitions (selected randomly), we assign random errors with values between 0.1 and 0.2 mag in step (b).

Figure 12 shows the ratio of light curves classified as linear (+) to those classified as linear (−) as a function of $t_{\rm decay}/t_{\rm rise}$ (middle plot) and $t_{\rm rise}$ (bottom plot). The figure shows that, to get linear (+) to linear (−) ratios similar to our results, we require the existence of outbursts with $2000 < t_{\rm rise} < 5000$ days and for $t_{\rm decay}$ to lie between about twice and 5 times the value of $t_{\rm rise}$. Light curves with equal values for the rise and decay of the outburst tend to produce an equal number of linear (+) and linear (−) objects, while larger values of $t_{\rm decay}$ compared with $t_{\rm rise}$ tend to overproduce linear (−) objects.

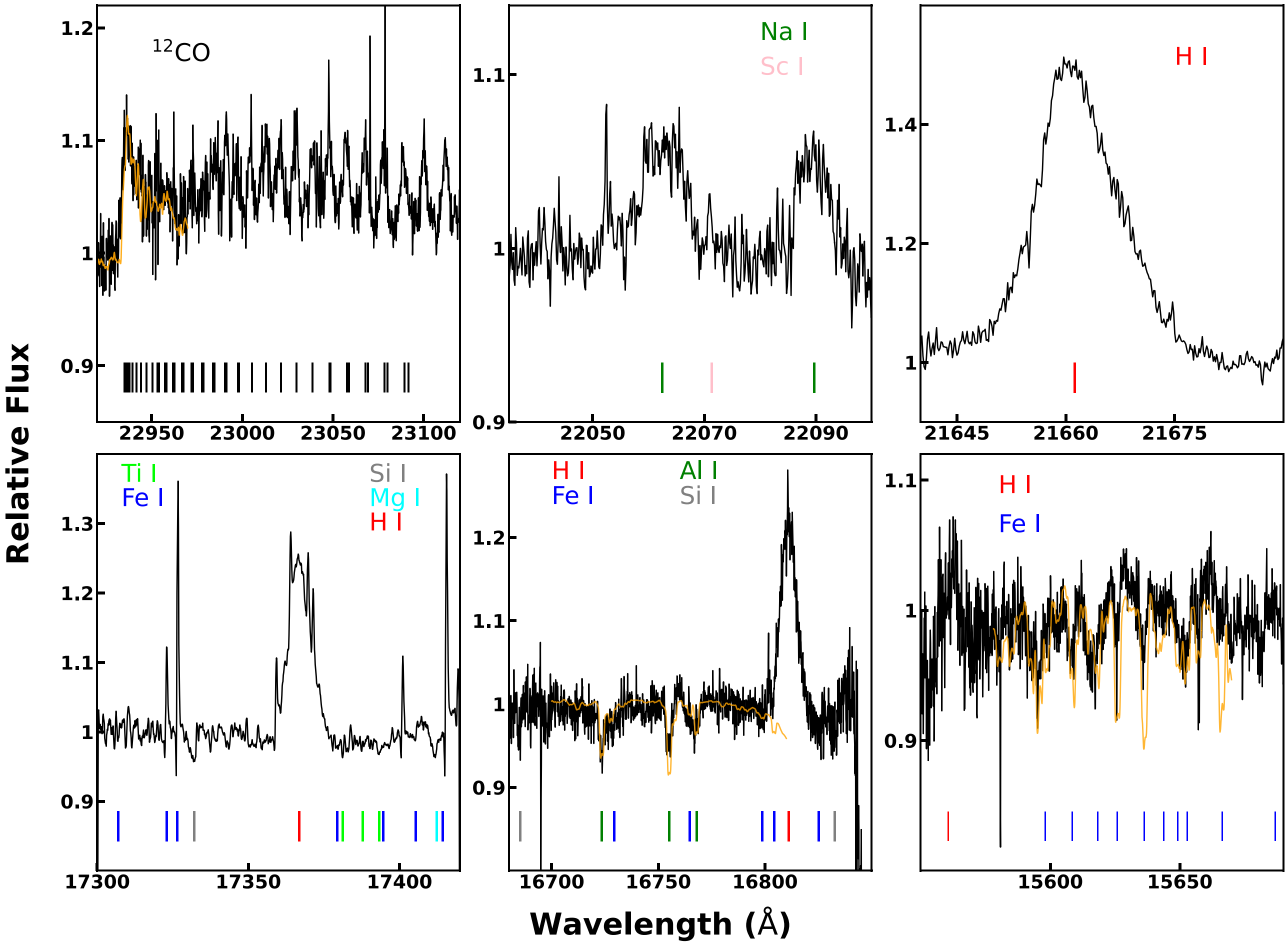

Figure 10. IGRINS spectra covering regions in the H and K bands for SPICY 21349. In the plot, we mark the wavelengths of transition lines from several elements. The orange solid line shows the result of convolving stellar templates with a Keplerian rotation model.

Examples of known FUors with $t_{\rm rise} > 2000$ days are rare. Recently, M. Ashraf et al. (2024) identified the YSO SSTgbs J21470601+4739394 as an FUor outburst of a $\simeq 0.2 M_\odot$ star. The mid-IR light curve of the source shows a slow rise over the 10 yr monitoring of WISE/NEOWISE observations. The classical FUor V1515 Cyg took 30 yr to reach its peak brightness (G. H. Herbig 1977; Z. M. Szabó et al. 2022). The existence of decades-long rises is interesting, as according to the models by J. Cleaver et al. (2023), such long mid-IR rises are expected in the outbursts reaching the largest accretion rates. In this sense, it is important to continue monitoring these sources (such as SPICY 41259; see Figure 13).

The values of $t_{\rm rise}$ and $t_{\rm decay}/t_{\rm rise}$ found from our sample can also provide a "typical" timescale of an FUor outburst. If we assume that $5000 > t_{\rm rise} > 2000$ days and $6 > t_{\rm decay}/t_{\rm rise} > 2.5$, then we find outburst durations that vary from 19 to 95 yr, with a mean of 48 yr.

6.2. Comparison with the Frequency of FUor Outbursts

The frequency of outbursts at different stages of YSO evolution has been measured through the detection of FUors in optical, near-, and mid-IR surveys (A. Scholz et al. 2013; C. Contreras Peña et al. 2019; W. Park et al. 2021; W. Zakri et al. 2022) as well as through an analysis of the chemical imprint left by outbursts (J. K. Jørgensen et al. 2015; T.-H. Hsieh et al. 2019). These methods all roughly agree on the increase in the recurrence timescales, τ, as the systems evolve. The frequency of bursts is estimated as once every $\tau = 112{,}000$ yr at the Class II stage (C. Contreras Peña et al. 2019), $\tau = 1750$–$10{,}000$ yr at the Class I stage (A. Scholz et al. 2013; T.-H. Hsieh et al. 2019; C. Contreras Peña et al. 2024), and $\tau = 490$–2000 yr at the Class 0 stage (W. J. Fischer et al. 2019; W. Park et al. 2021; W. Zakri et al. 2022).

We can use the estimates of τ presented above to give a rough estimate of the mean lifetime of FUor outbursts. Setting $\tau = 2000$, 10,000, and 112,000 yr for the Class I, FS, and Class II stages, respectively, we expect to observe 5×10^{-4}, 10^{-4}, and 8.9×10^{-6} outbursts per star per year at the different stages. Given the sample sizes at each evolutionary stage (see Section 2.1), we then determine that we should observe roughly 7.9, 2.4, and 0.5 new outbursts per year in Class I, FS, and Class II stages, respectively, or $\sim$11 outbursts per year in the overall SPICY sample.

Given the above yearly rate of new burst detection for the SPICY sample estimated using literature-based recurrence timescales, along with the 717 monitored on-going FUors (assuming that the 717 *linear* sources are indeed FUor outbursts), we estimate that the typical time that each FUor source must spend in an observable burst mode is $717/11 \simeq 65$ yr. This number is affected upward by contamination and downward by the fact that we may have missed some outbursts. The spectroscopic sample shows a 10% contamination from evolved sources. This sample is biased toward the

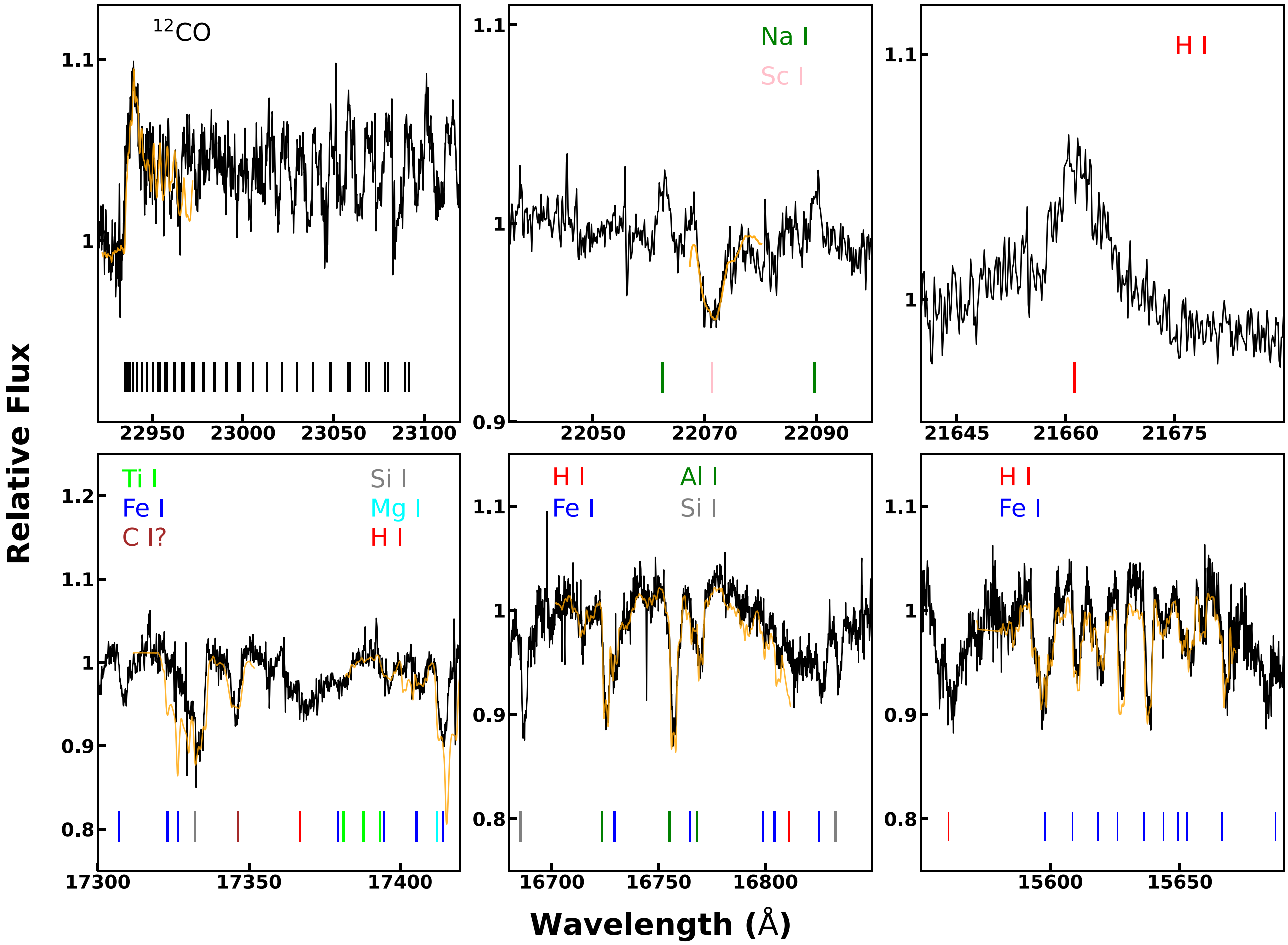

Figure 11. IGRINS spectra covering regions in the *H* and *K* bands for SPICY 42901. In the plot, we mark the wavelengths of transition lines from several elements. The orange solid line shows the result of convolving stellar templates with a Keplerian rotation model.

brightest end of the distribution of candidate FUors, and therefore, the 10% may be a lower limit of the contamination level. If we assume that contamination can reach as high as 3 times this level, then the number of candidates reduces to ∼500 sources. A rough estimate of the number of outbursts we are missing can be derived from the number of times a "typical" synthetic light curve of an outburst would not be classified as a linear source. Based on the results from the previous section, we create a synthetic light curve with an amplitude of 2.4 mag, $t_{\rm rise} = 2000$ days, and $t_{\rm decay}/t_{\rm rise} = 6.5$. We then followed steps (a)–(d) from the simulations of the previous section. We find that this outburst is classified as linear in 59% of the 2000 repetitions. This would imply that the number of outbursts in our sample (after considering the 10% lower limit of the contamination) could be as high as ∼1100 sources.

The outbursting FUor range of $500 < N_{\rm events} < 1100$ implies a mean-burst lifetime between 45 and 100 yr. Although there are many caveats that affect how we realize this number, the ranges of values for the mean-burst lifetime are fairly consistent with the "typical" duration of outbursts found above in Section 6.1, as well as with the longest baselines we are able to retrieve from the SuperCOSMOS survey in Section 4.4.

Theoretical models that study the processes that lead to an outburst predict a wide range of durations (see Figure 7 in M. Audard et al. 2014). Stellar flybys can lead to outbursts lasting decades to centuries (E. M. A. Borchert et al. 2022). Planet-induced accretion events, and sudden triggering of magnetorotational instabilities (MRI) in the inner disk can lead to durations typically lower than 60 yr (G. Lodato & C. J. Clarke 2004; J. Cleaver et al. 2023). In general, gravitational instabilities (GI) that lead to disk fragmentation or that trigger MRI predict the largest durations (up to 500 yr; E. I. Vorobyov 2009; K. Kadam et al. 2020; J. Cleaver et al. 2023). Some outbursts that occur due to disk fragmentation at the end of the embedded phase/early Class II stage also show durations of a few decades (E. I. Vorobyov 2009).

The mean-burst values derived from our analysis are inconsistent with the centuries-long timescales predicted by some of the models. However, the instabilities that lead to such long timescales are triggered during stages of large mass infall rates from the envelope. These large rates are associated with the deeply embedded Class 0 stage of YSO evolution. The SPICY catalog is dominated by Class II and FS YSOs; therefore, the mean-burst values derived above may indicate that GI is not the dominant mechanism leading to outbursts in this sample.

7. Summary

In this work, we have attempted to discover YSOs that (1) have gone into an outburst prior to the start of modern monitoring or (2) show long-term slow-rising outbursts. For

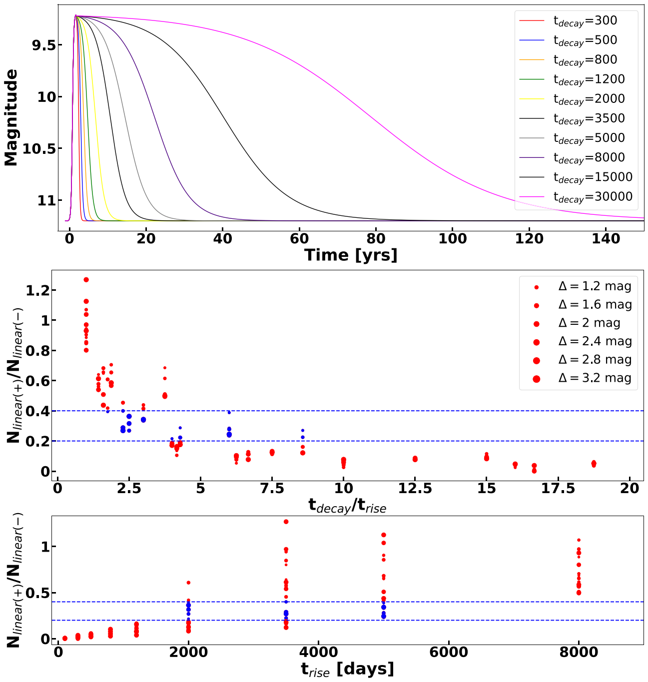

Figure 12. (Top) Synthetic FUor light curves for $t_{\rm rise} = 300$ days, amplitude of 2 mag, and for different decay timescales of the outburst. (Middle, bottom) Ratio of rising (linear $(+)$) to fading (linear $(-)$) objects as a function of $t_{\rm decay}/t_{\rm rise}$ (middle plot) and $t_{\rm rise}$ (bottom plot). In both figures, the size of the circles increases with the amplitude of the outburst. Blue circles mark the results that yield linear $(+)$ to linear $(-)$ between 0.2 and 0.4. These regions are also marked by dashed blue lines.

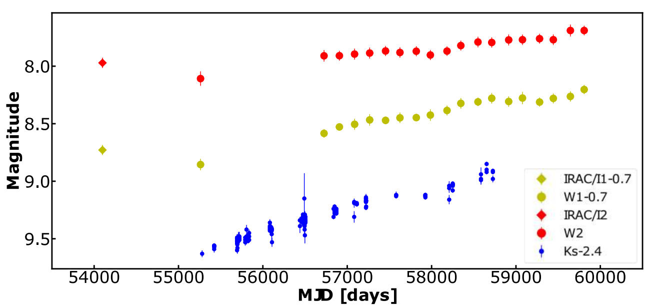

Figure 13. Near- to mid-IR light curve of SPICY 41259.

this, we have used several properties of accretion-related outbursts. Both types of outburst should be well fitted by linear models as they are either slowly declining after an outburst (S. J. Kenyon et al. 2000) or slowly rising toward peak brightness (M. Ashraf et al. 2024). Further, the YSOs that go into an outburst should reach a similar location in mid-IR CMDs, independent of the mass of the central star (H. Liu et al. 2022). Finally, the near-IR spectra of these sources should show the characteristics of FUors, e.g., ^{12}CO absorption broadened by disk rotation (M. S. Connelley & B. Reipurth 2018).

We analyzed the WISE/NEOWISE mid-IR light curves of 99,702 YSOs arising from the SPICY catalog (M. A. Kuhn et al. 2021). Classification of their light curves using the methods from W. Park et al. (2021) allowed us to find 717 YSOs with light curves that are well fitted by a linear model, 526 with a negative slope, and 191 with a positive slope. Using additional data from near-IR (VVV) data, as well as the location of these objects in W1 versus W1 − W2 CMDs, we are able to determine candidates with a higher probability of being FUors.

Based on the results from YSOs with spectroscopic data (data obtained by our group, as well as data from the literature), the method outlined in this work is found to be highly successful in finding eruptive YSOs in the long-term WISE/NEOWISE data. We confirm that 18 out of 20 objects are eruptive variable YSOs. In only two objects, we find spectroscopic evidence that points to an evolved nature of these sources. The eruptive variable YSOs can be divided into four bona fide FUors (as a high-amplitude outburst has been observed in the past), eight FUor-like sources (no outburst has been recorded), and six peculiar sources (show a mix of characteristics from the known subclasses of eruptive YSOs). Nine of the YSOs analyzed in this work correspond to new additions to the variable class (seven FUor-like, two peculiar). For a more detailed discussion of the classes of eruptive variable YSOs, see M. Audard et al. (2014), M. S. Connelley & B. Reipurth (2018), and C. Contreras Peña et al. (2023b).

The spectra of 12 objects show a lack of emission lines and have strong absorption from ^{12}CO. In six cases, the FUOr classification arises from midresolution spectra (M. S. Connelley & T. P. Greene 2010; C. Contreras Peña et al. 2023a; Z. Guo et al. 2024a), and our mid-IR light curves support this classification. In six sources, we have high-resolution IGRINS spectra ($R \sim 45{,}000$) that show broadened absorption that can be fitted by convolving stellar templates with a Keplerian disk rotation profile. We also observe an increase in velocity with a wavelength that is expected in the accretion disk of FUors. Contamination from D-type symbiotic sources is discarded as our sample does not show the Hα excess (estimated from broadband photometry) that is expected in these evolved systems.

In six sources, we find ^{12}CO, Brγ, and Na I in emission. These features are generally not attributed to the more extreme and longer duration outbursts (a.k.a. FUors), which could argue against these sources being in a high-accretion state from a centuries-long outburst. However, there is an increasing number of eruptive YSOs that show long-duration outbursts and an emission line spectrum during the high state (J. Eisloeffel et al. 1991; C. Contreras Peña et al. 2017a; Z. Guo et al. 2021). In these cases, magnetospheric accretion would still be in control even at large accretion rates (Z. Guo et al. 2021). The latter could be due to these YSOs having larger masses of the central star (N. Calvet et al. 1991; H. Liu et al. 2022). The mechanism driving the variability is likely still a large disk instability.

In the particular case of SPICY 42901, we also observe that the H-band spectrum is dominated by broad absorption of Fe I and Al I and a lack of hydrogen emission. It is possible that the multiple components arise from different regions of the disk, with the hot midplane dominating the emission in the inner regions (leading to absorption in the H band), while CO emission arises from regions where the atmosphere of the disk has a larger temperature than the midplane. However, we could also be observing the combined flux in a binary system. For example, Z CMa is a binary system comprised of a Herbig Ae/Be star and an FUor, with the ^{12}CO emission arising from the higher-mass object and the FUor dominating the flux at shorter wavelengths (see, e.g., B. A. Whitney et al. 1993; S. Hinkley et al. 2013; M. Bonnefoy et al. 2017).

The overall number of linear (+) and linear (−) objects provides some insights into the timescales involved in accretion-driven outbursts. First, we performed a Monte Carlo simulation of synthetic light curves of various amplitudes, rising and decay timescales to estimate the parameters that would lead to the observed ratio of linear (+) to linear (−) objects in our sample. The simulation yields that outburst decay times must be at least 2.5 times longer than the rise times. In addition, a population of outbursts with rise timescales between 2000 and 5000 days must exist to get our observed number of linear (+) YSOs. Using these results, we also estimate that a "typical" outburst can last between 19 and 95 yr, with a mean duration of 48 yr. Second, we used previously measured values of the frequency of outbursts and determined that, to detect between 500 and 1100 outbursts in the SPICY sample, FUor outbursts must have a mean-burst lifetime of between 45 and 100 yr. Both analyses yield consistent results in terms of outburst duration, and both agree with the longest baselines we are able to retrieve for our spectroscopic sample.

Future observations of the sample of 717 YSOs presented in this paper have the potential to uncover a large number of YSO outbursts.

Acknowledgments

C.C.P. was supported by the National Research Foundation of Korea (NRF) grant funded by the Korean government (MEST; No. 2019R1A6A1A10073437). D.J. is supported by NRC Canada and by an NSERC Discovery Grant. This work was supported by the New Faculty Startup Fund from Seoul National University and the NRF grant funded by the Korean government (MSIT; grant Nos. 2021R1A2C1011718 and RS-2024-00416859). This work was supported by K-GMT Science Program (PID: GS-2023A-Q-207) of Korea Astronomy and Space Science Institute (KASI). Z.G. is supported by the ANID FONDECYT Postdoctoral program No. 3220029, the ANID Millennium Science Initiative, AIM23-0001, and is supported by the China-Chile Joint Research Fund (CCJRF No.2301) and Chinese Academy of Sciences South America Center for Astronomy (CASSACA) Key Research Project E52H540301. G.J.H. is supported by the National Key R&D program of China 2022YFA1603102 and by general grant 12173003 from the National Natural Science Foundation of China. P.W.L. acknowledges support by grant ST/Y000846/1 of the UK Science and Technology Facilities Council.

This research has made use of the NASA/IPAC Infrared Science Archive, which is funded by the National Aeronautics and Space Administration and operated by the California Institute of Technology. This work used the Immersion Grating Infrared Spectrometer (IGRINS) that was developed under a collaboration between the University of Texas at Austin and the Korea Astronomy and Space Science Institute (KASI) with the financial support of the US National Science Foundation 27 under grants AST-1229522 and AST-1702267, of the University of Texas at Austin, and of the Korean GMT Project of KASI. This work is based on observations obtained at the international Gemini Observatory, a program of NSF NOIRLab, which is managed by the Association of Universities for Research in Astronomy (AURA) under a cooperative agreement with the U.S. National Science Foundation on behalf of the Gemini Observatory partnership: the U.S. National Science Foundation (United States), National Research Council (Canada), Agencia Nacional de Investigación y Desarrollo (Chile), Ministerio de Ciencia, Tecnologìa e Innovación (Argentina), Ministério da Ciência, Tecnologia, Inovações e Comunicações (Brazil), and Korea Astronomy and Space Science Institute (Republic of Korea).

Facilities: IRTF (SpeX medium-resolution spectrograph), WISE, Gemini:South (IGRINS high-resolution spectrograph).

Appendix
Sources

In this section, we provide some additional information about the SPICY objects with a spectroscopic follow-up. Table 3 contains the values for the spectral index and distance found in the literature for the 20 sources.

SPICY 11492. Designated L222_1 in Z. Guo et al. (2024a), this source is classified as an FUor based on the spectroscopic and photometric characteristics of the YSO.

This is a Class II YSO in SPICY ($\alpha = -0.74$); however, Z. Guo et al. (2024a) determine $\alpha = 0.82$, and P. W. Lucas et al. (2024) finds $\alpha = 0.47$, which would place it in the Class I YSO category. The difference in classification arises as M. A. Kuhn et al. (2021) derives α from the [4.5] − [8.0] color of the source, while Z. Guo et al. (2024a) and P. W. Lucas et al. (2024) derive the slope from the infrared SED of the source. The difference among the latter arises as Z. Guo et al. (2024a) include the VVV 2.15 μm observation, while P. W. Lucas et al. (2024) uses wavelengths longer than $3 > \mu$m, in order to reduce the effect of foreground interstellar extinction.

M. A. Kuhn et al. (2021) searched for spatial clustering among their sample of YSOs. SPICY 11492 is found to be associated with group G295.0−0.6, which is comprised of 132 YSOs, 31 of which have five-parameter Gaia astrometric solutions. The median parallax of 0.319 ± 0.063 mas yields a distance of $d = 1.64^{+0.19}_{-0.15}$ kpc. Z. Guo et al. (2024a) also provides two values of distance for the source. The first one is from a possible spatial association with SFRs ($d_{\rm SFR} = 9.6$ kpc), and a second value is from the radial velocity measurement of the CO bandhead absorption ($d_{\rm RV} = 10.2$ kpc).

SPICY 15180. This source corresponds to Stim 1 in Z. Guo et al. (2021), a YSO classified as an emission line eruptive YSO in that work. The authors provide a Class I YSO classification given $\alpha = 0.63$. A similar classification is derived from $\alpha = 0.31$ estimated by P. W. Lucas et al. (2024). This differs from the FS ($\alpha = 0.16$) classification given by M. A. Kuhn et al. (2021). The difference arises from using different methods in these works. The only distance information for the source arises from the radial velocity measurement, with $d_{\rm RV} = 10.5$ kpc.

SPICY 15470. This object is a Class II YSO in the SPICY catalog. Prior to this classification, the object was part of the T. P. Robitaille et al. (2008) sample of intrinsically red objects from Spitzer. The object was classified as a candidate AGB star as it showed $[8.0] - [24] < 2.5$ mag.

In the search for spatial clustering, SPICY 15470 is found to be associated with group G304.0+02. The latter is comprised of 201 YSOs, 35 of which have five-parameter Gaia astrometric solutions. The median parallax of 0.379 $\pm$ 0.047 mas yields a distance of $d = 3.06^{+0.51}_{-0.39}$ kpc.

SPICY 21349. This object is a Class II YSO in the SPICY catalog. This source has also been classified as a candidate

Table 3
Information on Classification and Distance for the 20 SPICY YSO Candidates with Spectroscopic Data

SPICY ID	Other Name	α[a]	α[b]		D[c] (kpc)	D[d] (kpc)	D[e] (kpc)
SPICY 11492	L222_1	−0.74	0.82	0.47	1.7	9.6	10.2
SPICY 15180	Stim 1	0.16	0.63	0.31	…	…	10.5
SPICY 15470	2MASS J13012070−6220014	−1.42	…	…	3.06	…	…
SPICY 21349	2MASS J14124874−6122507	−0.40	…	…	3.54	…	…
SPICY 29017	VVVv631	−0.51	−0.14	…	1.5	2.3	…
SPICY 31759	L222_33	−0.38	0.39	−0.28	…	3.4	4.2
SPICY 35235	…	−0.95	…	…	…	…	…
SPICY 36590	VVVv270	0.13	1.8	0.26	…	2.3	4.6
SPICY 42901	2MASS J16515774−4542390	−0.14	…	…	2.33	…	…
SPICY 57130	2MASS J17342304−3052235	−0.54	…	…	…	…	…
SPICY 63130	L222_148	1.85	1.67	…	1.5	9.1	8.3
SPICY 65417	2MASS J17482632−2407330	−0.82	…	…	7.39	…	…
SPICY 68600	2MASS J17550099−2801273	−0.80	…	…	4.29	…	…
SPICY 68696	2MASS J17551531−2852581	−1.00	…	…	6.96	…	…
SPICY 87984	IRAS 18341−0113N	0.81	0.91	…	0.59	…	…
SPICY 95397	SSTGLMC G035.3429-00.4212	−0.67	…	…	1.2	…	…
SPICY 99341	2MASS J19113876+0902592	−0.41	−0.31	…	2.9	3	…
SPICY 100587	2MASS J19171791+1116323	−0.33	…	…	…	…	…
SPICY 109102	…	−0.30	…	…	…	…	…
SPICY 111302	…	−1.44	…	…	2.2	…	…

Notes.
[a] Spectral index from SPICY.
[b] Spectral index from the literature. See main text for details.
[c] Distance from mean parallaxes of stellar associations found in SPICY.
[d] Distance from spatial association with star-forming regions located within 5′ from the YSO (see C. Contreras Peña et al. 2017b).
[e] Distance from radial velocity measurement of the CO bandhead absorption.

YSO in previous works (T. P. Robitaille et al. 2008; G. Marton et al. 2016, 2019), but fails to be classified as a pre-main-sequence star in M. Vioque et al. (2020). This source has been observed with Gaia, where a parallax of 0.84 ± 0.42 mas is presented in the Gaia DR3 (Gaia Collaboration et al. 2023). This yields a distance of $d = 1.27^{1.45}_{-0.44}$ kpc. The object is also associated with group G311.8−0.0 in M. A. Kuhn et al. (2021), a cluster with 1374 members, 209 of which have full Gaia astrometric solutions. This provides a median parallax of 0.335 ± 0.042 mas, or a distance of $d = 3.54^{+0.51}_{-0.46}$ kpc. Given the large uncertainties in the Gaia parallax of the source, we argue in favor of the distance estimated to the SPICY group G311.8−0.0 as the distance of SPICY 21349.

SPICY 29017. This is VVVv631, an eruptive YSO with an emission line spectrum (C. Contreras Peña et al. 2017a; Z. Guo et al. 2020). Different methods yield a classification of this source from Class II ($\alpha = -0.5$) in SPICY to FS ($\alpha = -0.14$) in C. Contreras Peña et al. (2017a).

M. A. Kuhn et al. (2021) find this source to be associated with group G326.6+0.6, a cluster with 405 members, 54 of which have full Gaia astrometric solutions. This provides a median parallax of 0.400 ± 0.045 mas, or a distance of $d = 2.3^{+0.3}_{-0.2}$ kpc. The latter agrees well with the distance to a close SFR provided in C. Contreras Peña et al. (2017a) of $d_{\rm SFR} = 2.3$ kpc.

SPICY 31759. This is source L222_33 in Z. Guo et al. (2024a) and P. W. Lucas et al. (2024). It was classified as an FUor based on its long-duration, high-amplitude ($\Delta K_s > 4.2$ mag) outburst, as well as the characteristics of its near-IR spectrum. This is a Class II YSO in the SPICY catalog ($\alpha = -0.38$), an FS source from $\alpha = -0.28$ in P. W. Lucas et al. (2024), while Z. Guo et al. (2024a) determine $\alpha = 0.39$, placing it in the Class I YSO category. Once again, the difference in classification arises from the different methods used to determine α.

Z. Guo et al. (2024a) provides a distance of 3.4 kpc (from distance to SFRs located within 5′ of the source) and 4.2 ± 0.5 kpc (from radial velocity measurement of the CO bandhead absorption).

SPICY 35235. This is a Class II YSO in the SPICY catalog. There is no previous information in the literature about this source.

SPICY 36590. This is source VVVv270 in C. Contreras Peña et al. (2017b, 2017a) and Z. Guo et al. (2020). This source is classified as an MNor, or eruptive YSO with mixed characteristics between FUors and EX Lupi–type objects, as it shows a long-duration outburst, but displays spectra dominated by emission lines. Due to the different methods used to determine a value of the spectral index, α, this source is classified as an FS YSO in SPICY and P. W. Lucas et al. (2024), and as a Class I YSO in C. Contreras Peña et al. (2017a). From radial velocity measurements, C. Contreras Peña et al. (2017a) determines a distance of 4.6 kpc to the source.

SPICY 42901. Classified as an FS source in SPICY, this object has been previously classified as a YSO candidate in T. P. Robitaille et al. (2008) and G. Marton et al. (2016). The source is part of the G339.9−1.0 group, which contains 121 members with 11 of them having full Gaia astrometric solutions. The mean parallax of these 11 sources provides a distance of $d = 2.33^{+1.92}_{-0.72}$ kpc.

SPICY 57130. This object shares similarities with SPICY 15470 as it is also a Class II YSO in the SPICY catalog, and it was also classified as a candidate AGB star in T. P. Robitaille et al. (2008) given that the values of its [8.0] − [24] color are lower than 2.5 mag. There is no available distance information for this object.

SPICY 63130. This is source L222_148 in Z. Guo et al. (2024a) where it is classified as an emission line eruptive YSO. The spectral index of the source in both Z. Guo et al. (2024a) and M. A. Kuhn et al. (2021) is consistent with that of a Class I YSO.

The source is part of the G0.2–0.1 group, which contains 3662 members with 194 of them having full Gaia astrometric solutions. The mean parallax of these sources (plx = 0.407 ± 0.043) provides a distance of $d = 2.2^{+0.2}_{-0.2}$ kpc. This differs from the distances provided by Z. Guo et al. (2024a) of $d_{\rm SFR} = 9.1$ kpc and $d_{\rm RV} = 8.3$ kpc.

SPICY 65417. This is a Class II YSO, with no group association in the SPICY catalog. It was also classified as a candidate YSO in G. Marton et al. (2019). The only information in distance arises from C. A. L. Bailer-Jones et al. (2021) with $d = 7.39^{+2.42}_{-2.06}$ kpc.

SPICY 68600. This Class II YSO from the SPICY catalog is also classified as a candidate YSO in G. Marton et al. (2019). This source is also part of the analysis of M. Vioque et al. (2020), where it is classified as a non-YSO. T. P. Robitaille et al. (2008) designates this object as a candidate AGB star due to its [8.0] − [24] color being lower than 2.5 mag. This object is not part of any clusters from the SPICY catalog. C. A. L. Bailer-Jones et al. (2021) provides a distance of $d = 4.29^{+4.05}_{-2.14}$ kpc.

SPICY 68696. This is a Class II YSO with no group association from the SPICY catalog. The object is also classified as a candidate YSO in G. Marton et al. (2019). This is also part of the sample of intrinsically ref objects of T. P. Robitaille et al. (2008) where it is classified as a candidate AGB star based on its [8.0] − [24] color. C. A. L. Bailer-Jones et al. (2021) provide a distance of $d = 6.96^{+2.84}_{-2.52}$ kpc.

SPICY 87894. IRAS 18341−0113N is part of the sample of M. S. Connelley & T. P. Greene (2010). It is classified as a Class I YSO in both M. S. Connelley & T. P. Greene (2010) and M. A. Kuhn et al. (2021).

The source is part of the G29.9+2.2 group, which contains 152 members with 36 of them having full Gaia astrometric solutions. The mean parallax of these sources (plx = 0.384 ± 0.074) provides a distance of $d = 2.4^{+0.4}_{-0.3}$ kpc. C. A. L. Bailer-Jones et al. (2021) provide a distance of $d = 0.59 \pm 0.06$ kpc.

SPICY 99341. This source was classified as an FUor in C. Contreras Peña et al. (2023a) due to the photometric and spectroscopic characteristics of the outburst. This is a Class II YSO ($\alpha = -0.31$) in the SPICY catalog (M. A. Kuhn et al. 2021). P. W. Lucas et al. (2017) include it in their sample of high-amplitude variables arising from the UKIDSS GPS survey (source 266, $\Delta K = 4$ mag). A distance of 3 kpc is estimated due to its possible association with the molecular cloud GRSMC 43.30−0.33 (R. Simon et al. 2001). C. A. L. Bailer-Jones et al. (2021) estimate a distance of $2.9^{+1.2}_{-1.1}$ kpc based on its Gaia parallax.

SPICY 95397. This source is classified as Class II YSO in SPICY. The observation of ^{13}CO $\Delta\nu = 2$ transition bandhead absorption is a clear indicator of the evolved nature of the source. The only distance information comes from the Gaia parallax of the source, with $d = 1.2 \pm 0.2$ kpc (C. A. L. Bailer-Jones et al. 2021).

SPICY 100587. This source is classified as an FUor in C. Contreras Peña et al. (2023a). This is a Class II YSO in SPICY. M. A. Kuhn et al. (2021) finds an association with group G45.8−0.4, a cluster with 78 sources. However, only one source has a full Gaia astrometric solution. Therefore, we prefer not to derive a distance based on this information.

SPICY 109102. This source is classified as an FS YSO in SPICY. We classified this source as FUor-like based on its IRTF/Spex spectrum. There is no distance information on this source.

SPICY 111302. This source is classified as Class II YSO in SPICY ($\alpha = -1.4$). The observation of ^{13}CO $\Delta\nu = 2$ bandhead emission is a clear indicator of the evolved nature of the source. The only distance information comes from the Gaia parallax of the source, with $d = 2.2 \pm 0.3$ kpc (C. A. L. Bailer-Jones et al. 2021).

ORCID iDs

Carlos Contreras Peña https://orcid.org/0000-0003-1894-1880
Jeong-Eun Lee https://orcid.org/0000-0003-3119-2087
Ho-Gyu Lee https://orcid.org/0000-0002-3808-7143
Gregory Herczeg https://orcid.org/0000-0002-7154-6065
Doug Johnstone https://orcid.org/0000-0002-6773-459X
Hanpu Liu https://orcid.org/0000-0003-2488-4667
Philip W. Lucas https://orcid.org/0000-0002-8872-4462
Zhen Guo https://orcid.org/0000-0003-0292-4832
Michael A. Kuhn https://orcid.org/0000-0002-0631-7514
Leigh C. Smith https://orcid.org/0000-0002-3259-2771
Jessy Jose https://orcid.org/0000-0003-4908-4404
Sung-Yong Yoon https://orcid.org/0000-0001-6216-0462
Sung-Chul Yoon https://orcid.org/0000-0002-5847-8096

References

Alonso-Garcìa, J., Mateo, M., Sen, B., et al. 2012, AJ, 143, 70
Andre, P., Ward-Thompson, D., & Barsony, M. 1993, ApJ, 406, 122
Ashraf, M., Jose, J., Lee, H.-G., et al. 2024, MNRAS, 527, 11651
Audard, M., Ábrahám, P., Dunham, M. M., et al. 2014, in Protostars and Planets VI, ed. H. Beuther et al. (Tucson, AZ: Univ. Arizona Press), 387
Bae, J., Hartmann, L., Zhu, Z., & Nelson, R. P. 2014, ApJ, 795, 61
Bailer-Jones, C. A. L., Rybizki, J., Fouesneau, M., Demleitner, M., & Andrae, R. 2021, AJ, 161, 147
Baluev, R. V. 2008, MNRAS, 385, 1279
Baraffe, I., Elbakyan, V. G., Vorobyov, E. I., & Chabrier, G. 2017, A&A, 597, A19
Becker, J. C., Batygin, K., & Adams, F. C. 2021, ApJ, 919, 76
Belczyński, K., Mikołajewska, J., Munari, U., Ivison, R. J., & Friedjung, M. 2000, A&AS, 146, 407
Bellm, E. C., Kulkarni, S. R., Graham, M. J., et al. 2018, PASP, 131, 018002
Benjamin, R. A., Churchwell, E., Babler, B. L., et al. 2003, PASP, 115, 953
Bonnefoy, M., Chauvin, G., Dougados, C., et al. 2017, A&A, 597, A91
Borchert, E. M. A., Price, D. J., Pinte, C., & Cuello, N. 2022, MNRAS, 517, 4436
Boss, A. P. 2013, ApJ, 764, 194
Bryan, G. R., Maddison, S. T., & Liffman, K. 2019, MNRAS, 489, 3879
Calvet, N., Patino, A., Magris, G. C., & D'Alessio, P. 1991, ApJ, 380, 617
Carlberg, J. K., Majewski, S. R., Patterson, R. J., et al. 2011, ApJ, 732, 39
Chambers, K. C., Magnier, E. A., Metcalfe, N., et al. 2016, arXiv:1612.05560
Cieza, L. A., Casassus, S., Tobin, J., et al. 2016, Natur, 535, 258
Cleaver, J., Hartmann, L., & Bae, J. 2023, MNRAS, 523, 5522
Cochetti, Y. R., Arias, M. L., Kraus, M., et al. 2021, A&A, 647, A164
Connelley, M. S., & Greene, T. P. 2010, AJ, 140, 1214
Connelley, M. S., & Reipurth, B. 2018, ApJ, 861, 145
Contreras Peña, C., Ashraf, M., Lee, J.-E., et al. 2023a, JKAS, 56, 253

Contreras Peña, C., Herczeg, G. J., Ashraf, M., et al. 2023b, MNRAS, 521, 5669
Contreras Peña, C., Lucas, P. W., Guo, Z., & Smith, L. 2024, MNRAS, 528, 1823
Contreras Peña, C., Lucas, P. W., Kurtev, R., et al. 2017a, MNRAS, 465, 3039
Contreras Peña, C., Lucas, P. W., Minniti, D., et al. 2017b, MNRAS, 465, 3011
Contreras Peña, C., Naylor, T., & Morrell, S. 2019, MNRAS, 486, 4590
Corradi, R. L. M., Rodrìguez-Flores, E. R., Mampaso, A., et al. 2008, A&A, 480, 409
Cushing, M. C., Vacca, W. D., & Rayner, J. T. 2004, PASP, 116, 362
Drew, J. E., Gonzalez-Solares, E., Greimel, R., et al. 2016, yCat, II/341, 0
Dunham, M. M., Stutz, A. M., Allen, L. E., et al. 2014, in Protostars and Planets VI, ed. H. Beuther et al. (Tucson, AZ: Univ. Arizona Press), 195
Eisloeffel, J., Guenther, E., Hessman, F. V., et al. 1991, ApJL, 383, L19
Enoch, M. L., Evans, N. J. I., Sargent, A. I., & Glenn, J. 2009, ApJ, 692, 973
Epchtein, N., de Batz, B., Copet, E., et al. 1994, Ap&SS, 217, 3
Evans, N. J., II, Dunham, M. M., Jørgensen, J. K., et al. 2009, ApJS, 181, 321
Fischer, W. J., Hillenbrand, L. A., Herczeg, G. J., et al. 2023, in ASP Conf. Ser. 534, Protostars and Planets VII, ed. S.-i. Inutsuka et al. (San Francisco, CA: ASP), 355
Fischer, W. J., Megeath, S. T., Tobin, J. J., et al. 2012, ApJ, 756, 99
Fischer, W. J., Safron, E., & Megeath, S. T. 2019, ApJ, 872, 183
Gaia Collaboration, Vallenari, A., Brown, A. G. A., et al. 2023, A&A, 674, A1
Gordon, K. D., Misselt, K. A., Bouwman, J., et al. 2021, ApJ, 916, 33
Greene, T. P., Wilking, B. A., Andre, P., Young, E. T., & Lada, C. J. 1994, ApJ, 434, 614
Gromadzki, M., Mikołajewska, J., Whitelock, P., & Marang, F. 2009, AcA, 59, 169
Guo, Z., Lucas, P. W., Contreras Peña, C., et al. 2020, MNRAS, 492, 294
Guo, Z., Lucas, P. W., Contreras Peña, C., et al. 2021, MNRAS, 504, 830
Guo, Z., Lucas, P. W., Kurtev, R., et al. 2024a, MNRAS, 528, 1769
Guo, Z., Lucas, P. W., Kurtev, R. G., et al. 2024b, MNRAS, 529, L115
Guo, Z., Lucas, P. W., Smith, L. C., et al. 2022, MNRAS, 513, 1015
Hajdu, G., Dékány, I., Catelan, M., & Grebel, E. K. 2020, ExA, 49, 217
Hambly, N. C., MacGillivray, H. T., Read, M. A., et al. 2001, MNRAS, 326, 1279
Hartmann, L., & Kenyon, S. J. 1996, ARA&A, 34, 207
Herbig, G. H. 1966, VA, 8, 109
Herbig, G. H. 1977, ApJ, 217, 693
Hillenbrand, L. A., Contreras Peña, C., Morrell, S., et al. 2018, ApJ, 869, 146
Hillenbrand, L. A., & Findeisen, K. P. 2015, ApJ, 808, 68
Hillenbrand, L. A., Miller, A. A., Carpenter, J. M., et al. 2019a, ApJ, 874, 82
Hillenbrand, L. A., Reipurth, B., Connelley, M., Cutri, R. M., & Isaacson, H. 2019b, AJ, 158, 240
Hinkle, K. H., Fekel, F. C., Joyce, R. R., et al. 2019, ApJ, 872, 43
Hinkley, S., Hillenbrand, L., Oppenheimer, B. R., et al. 2013, ApJL, 763, L9
Hodgkin, S. T., Harrison, D. L., Breedt, E., et al. 2021, A&A, 652, A76
Hsieh, T.-H., Murillo, N. M., Belloche, A., et al. 2019, ApJ, 884, 149
Hubbard, A. 2017, MNRAS, 465, 1910
Jayasinghe, T., Kochanek, C. S., Stanek, K. Z., et al. 2018, MNRAS, 477, 3145
Jørgensen, J. K., Visser, R., Sakai, N., et al. 2013, ApJL, 779, L22
Jørgensen, J. K., Visser, R., Williams, J. P., & Bergin, E. A. 2015, A&A, 579, A23
Kadam, K., Vorobyov, E., Regály, Z., Kóspál, Á., & Ábrahám, P. 2020, ApJ, 895, 41
Kenyon, S. J., Hartmann, L. W., Strom, K. M., & Strom, S. E. 1990, AJ, 99, 869
Kenyon, S. J., Kolotilov, E. A., Ibragimov, M. A., & Mattei, J. A. 2000, ApJ, 531, 1028
Kidder, B., Mace, G., López-Valdivia, R., et al. 2021, ApJ, 922, 27
Kraus, M., Arias, M. L., Cidale, L. S., & Torres, A. F. 2020, MNRAS, 493, 4308
Kuhn, M. A., de Souza, R. S., Krone-Martins, A., et al. 2021, ApJS, 254, 33
Kuhn, M. A., Saber, R., Povich, M. S., et al. 2023, AJ, 165, 3
Kunitomo, M., Guillot, T., Takeuchi, T., & Ida, S. 2017, A&A, 599, A49
Lada, C. J. 1987, in IAU Symp. 115, Star Forming Regions, ed. M. Peimbert & J. Jugaku (Cambridge: Cambridge Univ. Press), 1
Lawrence, A., Warren, S. J., Almaini, O., et al. 2007, MNRAS, 379, 1599
Lee, J.-E. 2007, JKAS, 40, 83
Lee, J.-E., Lee, S., Baek, G., et al. 2019, NatAs, 3, 314
Lee, J.-E., Lee, S., Lee, S., et al. 2021b, ApJL, 916, L20
Lee, J.-E., Park, S., Green, J. D., et al. 2015, ApJ, 807, 84
Lee, Y.-H., Johnstone, D., Lee, J.-E., et al. 2021a, ApJ, 920, 119
Liu, H., Herczeg, G. J., Johnstone, D., et al. 2022, ApJ, 936, 152
Lodato, G., & Clarke, C. J. 2004, MNRAS, 353, 841
Lomb, N. R. 1976, Ap&SS, 39, 447
Lorenzetti, D., Antoniucci, S., Giannini, T., et al. 2012, ApJ, 749, 188
Lucas, P. W., Elias, J., Points, S., et al. 2020, MNRAS, 499, 1805
Lucas, P. W., Hoare, M. G., Longmore, A., et al. 2008, MNRAS, 391, 136
Lucas, P. W., Smith, L. C., Contreras Peña, C., et al. 2017, MNRAS, 472, 2990
Lucas, P. W., Smith, L. C., Guo, Z., et al. 2024, MNRAS, 528, 1789
Mace, G., Sokal, K., Lee, J.-J., et al. 2018, Proc. SPIE, 10702, 107020Q
Mainzer, A., Bauer, J., Cutri, R. M., et al. 2014, ApJ, 792, 30
Mainzer, A., Grav, T., Bauer, J., et al. 2011, ApJ, 743, 156
Mairs, S., Lee, S., Johnstone, D., et al. 2024, ApJ, 966, 215
Marton, G., Ábrahám, P., Szegedi-Elek, E., et al. 2019, MNRAS, 487 2522
Marton, G., Tóth, L. V., Paladini, R., et al. 2016, MNRAS, 458, 3479
Minniti, D., Lucas, P., Emerson, J., et al. 2010, NewA, 15, 433
Moore, A. M., Kasliwal, M. M., Gelino, C. R., et al. 2016, Proc. SPIE, 9906, 99062C
Mundt, R., Stocke, J., Strom, S. E., Strom, K. M., & Anderson, E. R. 1985, ApJL, 297, L41
Najita, J., Carr, J. S., Glassgold, A. E., Shu, F. H., & Tokunaga, A. T. 1996, ApJ, 462, 919
Ochsenbein, F., Bauer, P., & Marcout, J. 2000, A&AS, 143, 23
Oksala, M. E., Kraus, M., Arias, M. L., et al. 2012, MNRAS, 426, L56
Onken, C. A., Wolf, C., Bessell, M. S., et al. 2019, PASA, 36, e033
Park, S., Lee, J.-E., Kang, W., et al. 2018, ApJS, 238, 29
Park, S., Lee, J.-E., Pyo, T.-S., et al. 2020, ApJ, 900, 36
Park, W., Lee, J.-E., Contreras Peña, C., et al. 2021, ApJ, 920, 132
Poorta, J., Ramìrez-Tannus, M. C., de Koter, A., et al. 2023, A&A, 676, A122
Rayner, J. T., Toomey, D. W., Onaka, P. M., et al. 2003, PASP, 115, 362
Reipurth, B., & Aspin, C. 1997, AJ, 114, 2700
Robitaille, T. P., Meade, M. R., Babler, B. L., et al. 2008, AJ, 136, 2413
Rodriguez, A. C., & Hillenbrand, L. A. 2022, ApJ, 927, 144
Saito, R. K., Hempel, M., Minniti, D., et al. 2012, A&A, 537, A107
Sandell, G., & Aspin, C. 1998, A&A, 333, 1016
Scargle, J. D. 1989, ApJ, 343, 874
Schechter, P. L., Mateo, M., & Saha, A. 1993, PASP, 105, 1342
Scholz, A., Froebrich, D., & Wood, K. 2013, MNRAS, 430, 2910
Semkov, E. H., Peneva, S. P., Munari, U., Milani, A., & Valisa, P. 2010, A&A, 523, L3
Simon, R., Jackson, J. M., Clemens, D. P., Bania, T. M., & Heyer, M. H. 2001, ApJ, 551, 747
Skrutskie, M. F., Cutri, R. M., Stiening, R., et al. 2006, AJ, 131, 1163
Smith, L. C., Lucas, P. W., Koposov, S. E., et al. 2025, MNRAS, 536, 3707
Smith, L. C., Lucas, P. W., Kurtev, R., et al. 2018, MNRAS, 474, 1826
Szabó, Z. M., Kóspál, Á., Ábrahám, P., et al. 2022, ApJ, 936, 64
Takagi, Y., Itoh, Y., Oasa, Y., & Sugitani, K. 2011, PASJ, 63, 677
Vioque, M., Oudmaijer, R. D., Schreiner, M., et al. 2020, A&A, 638, A21
Vorobyov, E. I. 2009, ApJ, 704, 715
Whitney, B. A., Clayton, G. C., Schulte-Ladbeck, R. E., et al. 1993, ApJ, 417, 687
Wright, E. L., Eisenhardt, P. R. M., Mainzer, A. K., et al. 2010, AJ, 140, 1868
Yoon, S.-Y., Lee, J.-E., Lee, S., et al. 2021, ApJ, 919, 116
Zakri, W., Megeath, S. T., Fischer, W. J., et al. 2022, ApJL, 924, L23
Zhu, Z., Hartmann, L., Calvet, N., et al. 2007, ApJ, 669, 483
Zwicky, L., Molyarova, T., Akimkin, V., et al. 2024, MNRAS, 527, 7652